Changes over time in the 100-year return value of climate model variables

Callum Leach[a], Kevin Ewans[b,c], Philip Jonathan[d,a,*]

[a]*Shell Information Technology International Ltd., London SE1 7NA, United Kingdom.*
[b]*MetOcean Research Ltd, New Plymouth 4310, New Zealand.*
[c]*Department of Infrastructure Engineering, University of Melbourne, Melbourne, VIC 3010, Australia.*
[d]*Department of Mathematics and Statistics, Lancaster University LA1 4YF, United Kingdom.*

Abstract

We assess the strength of evidence in favour of changes in the distributional tail characteristics of wind, solar irradiance and temperature variables available as output of CMIP6 climate models, due to climate forcing. We estimate global and climate zone annual maximum and annual mean data for the period (2015, 2100) from daily output of seven CMIP6 GCMs for the daily wind speed (`sfcWind`) and maximum wind speed (`sfcWindmax`), solar irradiance (`rsds`) and near-surface temperature (`tas`) variables. We also calculate the corresponding annualised data for individual locations within neighbourhoods of the North Atlantic and Celtic Sea region. For each data source we access output corresponding to three climate scenarios and multiple climate ensemble runs. We then estimate non-stationary extreme value models (GEVR) for annual extremes, and perform non-homogeneous Gaussian regression (NHGR) for annual means, using Bayesian inference. We use the estimated statistical models to quantify the distribution of (i) the change in the 100-year return value for annual extremes, and (2) the change in annual mean level, over the period (2025, 2125). To summarise results, we estimate linear mixed effects models for the observed variation of (i) and (ii). Evidence for changes in the 100-year return value for annual maxima of wind variables over time and with climate scenario is weak, in marked contrast to our findings for `rsds` and `tas`. For annual means, there is stronger evidence for changes over time for wind variables, especially in the Northern Hemisphere, but the extent of the changes is small.

Keywords: structural design; climate; CMIP6; wind speed; Bayesian inference; return value; generalised extreme value; non-homogeneous Gaussian regression; linear mixed effects model;

1. Introduction

The Summary for Policymakers from the 6th assessment report of the Intergovernmental Panel on Climate Change (IPCC 2021) states unequivocally that human activity has warmed the Earth, resulting in changes to the atmosphere and oceans in particular. It is likely that global average precipitation has increased, that near-surface ocean salinity patterns have changed, that global mean sea level has increases, that mid-latitude storm tracks have shifted poleward, that sea ice has retreated in the Arctic (but not in the Antarctic), and that the surface of the Greenland Ice Sheet has melted, all due to human activity. The rate of occurrence of temperature extremes has increased, as has that of Category 3-5 tropical cyclones, as a result of human activity.

Numerous numerical studies (e.g. Young and Ribal 2019, Meucci et al. 2020, Meucci et al. 2022, Ewans and Jonathan 2023) reporting likely changes in wind and wave climate, have been summarised in Ewans and Jonathan (2023). Most historical studies are based on global or regional analysis of output from Coupled Model Intercomparison Project (CMIP) General Circulation Models (GCMs). Output is available from multiple institutions (including e.g. the UK Metoffice, the Norwegian Climate Centre, the Chinese Meteorological Administration and the Japanese Meteorological Research Institute) for a large set of climate variables. For the 6th phase of CMIP (CMIP6), daily values of climate variables are provided for the period 2015-2100, under different assumptions combining future Shared Socioeconomic Pathways (SSPs) and Representative Concentration Pathways (RCPs); see Section 2 for further details.

GCMs behave somewhat differently to each other, due to different modelling assumptions made (e.g. IPCC 2013, Chapter 8). Moreover, just as wave hindcast and forecast model output is generally calibrated (e.g. Sung and Tuo 2024) to provide better in-situ agreement with measurements, it is to be expected that GCM output should be calibrated similarly for better agreement with measurements (e.g. Bellprat et al. 2012, Lemos et al. 2023, Lavoie et al. 2024, Meucci et al. 2024). There is a difference however. For calibration of a hindcast, both hindcast and measurement

---

data are typically available for a relatively large proportion of the period of the hindcast. For calibration of short-term forecasts similarly, historical forecasts and corresponding measurements are both available over a relatively long period, with which to perform a reasonable calibration. For GCM output, by definition, the proportion of the total time interval of the GCM output for which measured data are available is relatively small, and focussed on the early years of GCM output by definition; specifically, for CMIP6 GCMs, there is no means by which we can be confident that a calibration developed for the years 2015-2024 would be appropriate in 2100. Nevertheless, we note the work of Tett et al. (2022) regarding reduction of GCM variability using calibration, and recently produced guidance (IOGP Report 662 2024) from the International Association of Oil and Gas Producers on potential climate change effects on metocean design and operating criteria.

Some authors (e.g. Severino et al. 2024, Waidelich et al. 2024) seek to couple the output of CMIP6 models with climate risk assessment models, to obtain predictions of future impacts (e.g. cost of damage to infrastructure). Severino et al. 2024 in particular emphasise the importance of incorporating climate model uncertainty in predictions. From the perspective of wind energy resources, Miao et al. (2023) find that wind speeds generally decrease under CMIP6 scenarios in the Northern Hemisphere; again, the variability in estimates due to climate model uncertainty is emphasised. Ibarra-Berastegui et al. (2023) find that climate-related changes in electricity generating capacity from wind and wave occur in at most 15% of coastal locations studied under CMIP6 SSP126 and SSP585 scenarios.

We are interested in assessing how informative CMIP6 output is regarding future extremes of climate variables. Specifically, how much consistency is there between predictions of extreme quantiles (e.g. the 100-year level) for variables such as solar irradiance, wind speed and temperature?

Objectives and outline

The objective of the current work is to examine key output from CMIP6 global coupled models at site-specific, regional and global scales, to form a view of what state-of-the-art science is telling us about climate change effects. We focus on assessing the change in extreme quantiles of annual distributions of climate variables, specifically the change in the 100-year return value for a climate variable over the next 100 years (from 2025 to 2125), for surface downwelling short wave radiation, near-surface wind speed, daily maximum near-surface wind speed and near-surface air temperature. For the global and climate zone analyses considered, we think it interesting to compare inferences for extremes with those for changes in the spatial means (e.g. global and climate zone averages) also.

The layout of the paper is as follows. The GCM output considered in the current study is introduced and summarised in Section 2, for both global and climate zone analysis (Section 2.1) and North Atlantic-Celtic Sea point location analysis (Section 2.2). Section 3 outlines the statistical methodology adopted to estimate the change in the 100-year return value for each climate variable over the next 100 years (i.e. the period 2025-2125), and changes in global and climate zone means over the same period. Extreme value analysis of annual maxima data is achieved by fitting non-stationary generalised extreme value (GEV) models, described in Section 3.1. Trends in spatial means over time are quantified using non-homogeneous Gaussian regression (NHGR, Section 3.2). Results of applying the models from Section 3 to the data from Section 2 are presented in Section 4. Section 4.1 provides a summary of the analysis for global annual extreme and mean data, Section 4.2 for climate zone annual extreme and mean data, and Section 4.3 for annual maxima from specific locations in the North Atlantic and Celtic Sea neighbourhoods. Discussions and conclusions are given in Section 5. Supporting illustrations are provided in the accompanying online Supplementary Material (SM), and referenced e.g. by Figure SM3. All data used in this work (global and climate zone annual maximum, minimum and mean data, and all North Sea and Celtic Sea annual maximum data) is accessible at Leach (2024). The software used for the analysis is provided at Leach and Jonathan (2024).

2. Global coupled model output

Output for 7 GCMs from CMIP6 was accessed via the UK Centre for Environmental Analysis (CEDA) archive during the Spring of 2024. For each of these GCMs, gridded output for the whole globe is generally available daily for the time period 2015-2100. We choose to examine annualised data for a total of 4 environmental variables of engineering interest: surface downwelling shortwave radiation ($\mathtt{rsds}$, Wm^{-2}), near-surface wind speed ($\mathtt{sfcWind}$, ms^{-1}), daily maximum near-surface wind speed ($\mathtt{sfcWindmax}$, ms^{-1}) and near-surface air temperature ($\mathtt{tas}$, K). In addition, we examine three climate scenarios (or climate experiments): SSP126, SSP245 and SSP585. Each of these scenarios combines a SSP with a RCP. Experiment SSP126 follows SSP1, a storyline with low climate change mitigation and adaptation challenges, and RCP2.6 which leads to (additional) radiative forcing of 2.6 Wm^{-2} by the year 2100. Analogously, experiment SSP245 (SSP585) follows SSP2 (SSP3), a storyline with intermediate (high) climate change mitigation and adaptation challenges, and RCP4.5 (RDC8.5) which leads to (additional) radiative forcing of 4.5 (8.5) Wm^{-2} by the year 2100.

Daily data are accessed directly from the CEDA archive. For `rsds`, `sfcWind` and `tas`, output corresponds to daily averages over higher-frequency underlying model time-steps over the past 24 hours. For `sfcWindmax`, the data corresponds to the maximum over higher-frequency model time-steps over the past 24 hours. Annual maxima are then extracted for each calendar year, and annual arithmetic means calculated, for all 4 climate variables; annual minima are also extracted per calendar year for `tas`.

Then, for each combination of GCM, climate scenario and variable, we examine output for five climate model ensemble members where available; these correspond to a common initialisation, physics and forcing per GCM, and are listed in Table 1. For each combination of GCM, climate scenario, variable and ensemble member, we therefore have access to four time-series each of 86 values of annual maximum, mean and `tas` minimum for the period 2015-2100, for each spatial grid location on the surface of the Earth.

GCM	Variable	SSP126	SSP245	SSP585
ACCESS-CM2 (AC)	rsds	r1i1p1f1, r4i1p1f1, r5i1p1f1	r1i1p1f1, r4i1p1f1, r5i1p1f1	r1i1p1f1, r4i1p1f1, r5i1p1f1
	sfcWind	r1i1p1f1, r2i1p1f1, r3i1p1f1, r4i1p1f1, r5i1p1f1	r1i1p1f1, r2i1p1f1, r3i1p1f1, r4i1p1f1, r5i1p1f1	r1i1p1f1, r2i1p1f1, r3i1p1f1, r4i1p1f1, r5i1p1f1
	sfcWindmax	r4i1p1f1, r5i1p1f1	r4i1p1f1, r5i1p1f1	r4i1p1f1, r5i1p1f1
	tas	r1i1p1f1, r2i1p1f1, r3i1p1f1, r4i1p1f1, r5i1p1f1	r1i1p1f1, r2i1p1f1, r3i1p1f1, r4i1p1f1, r5i1p1f1	r1i1p1f1, r2i1p1f1, r3i1p1f1, r4i1p1f1, r5i1p1f1
CAMS-CSM1-0 (CA)	tas	r2i1p1f1	r2i1p1f1	r2i1p1f1
CESM2 (CE)	sfcWind	r4i1p1f1, r10i1p1f1,r11i1p1f1	r4i1p1f1, r10i1p1f1,r11i1p1f1	r4i1p1f1, r10i1p1f1,r11i1p1f1
	tas	r4i1p1f1, r10i1p1f1,r11i1p1f1	r4i1p1f1, r10i1p1f1,r11i1p1f1	r4i1p1f1, r10i1p1f1,r11i1p1f1
	rsds	r4i1p1f1, r10i1p1f1,r11i1p1f1	r4i1p1f1, r10i1p1f1,r11i1p1f1	r4i1p1f1, r10i1p1f1,r11i1p1f1
EC-Earth3 (EC)	rsds	r1i1p1f1,r4i1p1f1	r1i1p1f1,r4i1p1f1	r1i1p1f1,r4i1p1f1
	sfcWind	r1i1p1f1,r4i1p1f1	r1i1p1f1,r4i1p1f1	r1i1p1f1,r4i1p1f1
	sfcWindmax	r1i1p1f1,r4i1p1f1	r1i1p1f1,r4i1p1f1	r1i1p1f1,r4i1p1f1
	tas	r1i1p1f1,r4i1p1f1, r9i1p1f1, r11i1p1f1	r1i1p1f1,r4i1p1f1, r9i1p1f1, r11i1p1f1	r1i1p1f1,r4i1p1f1, r9i1p1f1, r11i1p1f1
MRI-ESM2-0 (MR)	rsds	r1i1p1f1, r2i1p1f1, r3i1p1f1, r4i1p1f1, r5i1p1f1	r1i1p1f1, r2i1p1f1, r3i1p1f1, r4i1p1f1, r5i1p1f1	r1i1p1f1, r2i1p1f1, r3i1p1f1, r4i1p1f1, r5i1p1f1
	sfcWind	r1i1p1f1, r2i1p1f1, r3i1p1f1, r4i1p1f1, r5i1p1f1	r1i1p1f1, r2i1p1f1, r3i1p1f1, r4i1p1f1, r5i1p1f1	r1i1p1f1, r2i1p1f1, r3i1p1f1, r4i1p1f1, r5i1p1f1
	sfcWindmax	r1i1p1f1, r2i1p1f1, r3i1p1f1, r4i1p1f1, r5i1p1f1	r1i1p1f1, r2i1p1f1, r3i1p1f1, r4i1p1f1, r5i1p1f1	r1i1p1f1, r2i1p1f1, r3i1p1f1, r4i1p1f1, r5i1p1f1
	tas	r1i1p1f1, r2i1p1f1, r3i1p1f1, r4i1p1f1, r5i1p1f1	r1i1p1f1, r2i1p1f1, r3i1p1f1, r4i1p1f1, r5i1p1f1	r1i1p1f1, r2i1p1f1, r3i1p1f1, r4i1p1f1, r5i1p1f1
NorESM2-MM (No)	rsds	r1i1p1f1	r1i1p1f1, r2i1p1f1	r1i1p1f1
	sfcWind	r1i1p1f1	r1i1p1f1, r2i1p1f1	r1i1p1f1
	tas	r1i1p1f1	r1i1p1f1, r2i1p1f1	r1i1p1f1
UKESM1-0-LL (UK)	rsds	r1i1p1f2, r2i1p1f2, r3i1p1f2, r4i1p1f2, r8i1p1f2	r1i1p1f2, r2i1p1f2, r3i1p1f2, r4i1p1f2, r8i1p1f2	r1i1p1f2, r2i1p1f2, r3i1p1f2, r4i1p1f2, r8i1p1f2
	sfcWind	r1i1p1f2, r2i1p1f2, r3i1p1f2, r4i1p1f2, r8i1p1f2	r1i1p1f2, r2i1p1f2, r3i1p1f2, r4i1p1f2, r8i1p1f2	r1i1p1f2, r2i1p1f2, r3i1p1f2, r4i1p1f2, r8i1p1f2
	sfcWindmax	r1i1p1f2, r2i1p1f2, r3i1p1f2, r4i1p1f2, r8i1p1f2	r1i1p1f2, r2i1p1f2, r3i1p1f2, r4i1p1f2, r8i1p1f2	r1i1p1f2, r2i1p1f2, r3i1p1f2, r4i1p1f2, r8i1p1f2
	tas	r1i1p1f2, r2i1p1f2, r3i1p1f2, r4i1p1f2, r8i1p1f2	r1i1p1f2, r2i1p1f2, r3i1p1f2, r4i1p1f2, r8i1p1f2	r1i1p1f2, r2i1p1f2, r3i1p1f2, r4i1p1f2, r8i1p1f2

Table 1: Summary of global coupled model (GCM) output considered. A total of 7 GCMs are used, listed in alphabetical order together with two-letter acronym (column 1). For each GCM, up to four climate variables are used, depending on their availability (column 2), for each of three climate scenarios (row 1, columns 3-5). A total of up to 5 ensemble members are considered for each combination of climate variable and scenario, again depending on availability (columns 3-5).

2.1. Compilation of spatial summaries: global and climate zone data

We consider analysis of spatial maxima, minima and means of corresponding location-specific annual maximum, minimum and mean data, for spatial domains corresponding to the whole globe and its partition into 5 climatic zones. We also present analysis of annual maximum data for specific locations in the North Atlantic and the Celtic Sea neighbourhood; see Section 2.2.

Global annual maximum data are calculated over the complete set of global grid locations $\mathcal{G}$ available for each GCM. Thus, given annual maximum output $\{y(i,j)\}$ for year $i = 1, 2, ..., 86$ at grid location $j \in \mathcal{G}$, the global (spatial) maximum time series $\{y_{G,\max}(i)\}$, $i = 1, 2, ..., 86$ is extracted from the location-specific maximum using

$$y_{G,\max}(i) = \max_{j \in \mathcal{G}} \{y(i,j)\}. \tag{1}$$

In a similar fashion, we also calculate the annual maximum for each of the Antarctic, Temperate South, Tropical, Temperate North and Arctic climate zones, defined by the latitudinal intervals $(-90°, -66.5°)$, $(-66.5°, -23.5°)$, $(-23.5°, 23.5°)$, $(23.5°, 66.5°)$ and $(66.5°, 90°)$ respectively. This calculation is made using Equation 1 (with $\mathcal{G}$ replaced by $\mathcal{G}_k$), for the appropriate choice of set $\mathcal{G}_k$ of climate zone locations, $k = 1, 2, ..., 5$. For variable `tas`, it is also interesting to consider global and climate zone annual minimum time-series, which are calculated in the analogous fashion from location-specific annual minimum data.

Illustrations of global annual maximum time-series for 5 ensemble members of `sfcWindmax` and `tas` from `ACCESS-CM2` are given in the left and right hand panels of Figure 1. Colours distinguish climate scenarios: SSP126 (green), SSP245 (orange) and SSP585 (grey); and line styles distinguish individual ensemble member output. It is apparent that the
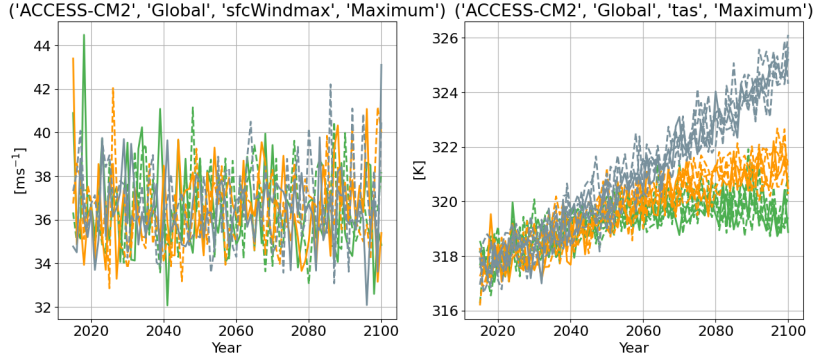
3

Figure 1: Illustrations of global annual maxima time-series for `sfcWindmax` (left) and `tas` (right) from `ACCESS-CM2`, for different climate scenarios (`SSP126`, green; `SSP245`, orange; `SSP585`, grey). Line styles distinguish different ensemble members.

effect of climate scenario is more pronounced for `tas` than for `sfcWindmax`. There is some evidence also under scenario `SSP126`, that global maximum `tas` asymptotes to a constant value with time (to around 320K for the `ACCESS-CM2` GCM illustrated in the right hand panel of Figure 1), and that perhaps `tas` under scenario `SSP245` asymptotes also (to around 322K); however similar trends are rarely seen for other climate variable, or for `tas` under `SSP585` for the period (2015,2100). Supporting illustrations for all other combinations of climate variables and GCMs are provided in Figure SM1 (of the SM); this figure also provides illustrations of generally reducing trends in global annual maximum `rsds`, and increasing trends in global annuam minimum of `tas`. Again, trends with time or the effect of climate scenario are difficult to discern for `sfcWind` and `sfcWindmax` relative to `tas` (in particular) and `rsds`.

We also calculate climate zone and global annual mean time-series from the corresponding location-specific annual mean data. To simplify the calculation per climate zone, we assume it reasonable to approximate the climate zone mean using the arithmetic mean over locations within the climate zone. With $\{y(i,j)\}$, $i = 1, 2, ..., 86$, $j \in \mathcal{G}_k$, $k = 1, 2, ..., 5$ now representing location-specific annual mean time-series per climate zone, the climate zone annual mean time-series is calculated using

$$y_{G_k,\text{mean}}(i) = \operatorname*{mean}_{j \in \mathcal{G}_k} \{y(i,j)\}. \tag{2}$$

We then estimate the global mean as a weighted average of climate zone means, with weight equal to the surface area $\mathcal{A}_k$, $k = 1, 2, ..., 5$ of the climate zone, using

$$y_{G,\text{mean}}(i) = \sum_k \mathcal{A}_k \ y_{G_k,\text{mean}}(i) \quad / \quad \sum_{k'} \mathcal{A}_{k'}. \tag{3}$$

Each climate zone surface area $\mathcal{A}_k$ is estimated assuming a spherical Earth. The resulting time-series of global annual mean data for the four climate variables are shown in Figure SM2. Obvious time trends and scenario effects are visible for `tas`; corresponding effects for `rsds` are clearer for global annual means than for global annual maxima (in Figure SM1). Regardless of GCM, `rsds` exhibits a positive slope in time under scenario `SSP126`, with more negative slope for `SSP245` and especially for `SSP585`; this results in a negative gradient for `rsds` under `SSP585` for three GCMs. `sfcWind` and `sfcWindmax` again show much weaker trends in time and with scenario; no scenario effect is discernable, but both `ACCESS-CM2` and `UKESM1-0-LL` GCMs (which share some modelling components) suggest a minor increase in `sfcWind` and `sfcWindmax` of approximately 0.1ms^{-1} over the 86 years. In contrast, `EC-Earth3` suggests that `sfcWind` and `sfcWindmax` reduce by the same amount in general over the same period.

Figure 2 illustrates time-series of annual maximum and minima data for the climate variables (rows) across climate zones (columns) for the `UKESM1-0-LL` GCM. To emphasise trends here, data have been smoothed using a moving $\pm$ 10-year median filter. Rows 1-4 represent annual maxima for `rsds`, `sfcWind`, `sfcWindmax` and `tas`, and row 5 annual minima of `tas`. Columns represent the Antarctic, Temperate South, Tropical, Temperate North and Arctic climate zones. Within each panel, colour distinguishes scenarios, and line style ensemble members, as described in the figure caption. Obvious differences in level are apparent across climate zones for all climate variables. Temporal trends are clearer for `tas` then for `rsds` than for `sfcWind` and `sfcWindmax`, although there are stronger time trends for `sfcWind` and `sfcWindmax` in the Arctic zone. Differences due to climate scenario are clearer for `tas` and then for `rsds` than for `sfcWind` and `sfcWindmax`. `rsds` shows a generally decreasing level across climate zones from the Antarctic. As would be expected due to reduced Coriolis effect, `sfcWind` and `sfcWindmax` are smaller in the Tropical zone. For `tas`, similar trends with climate zone are seen for both annual maxima and annual minima. The corresponding data (without

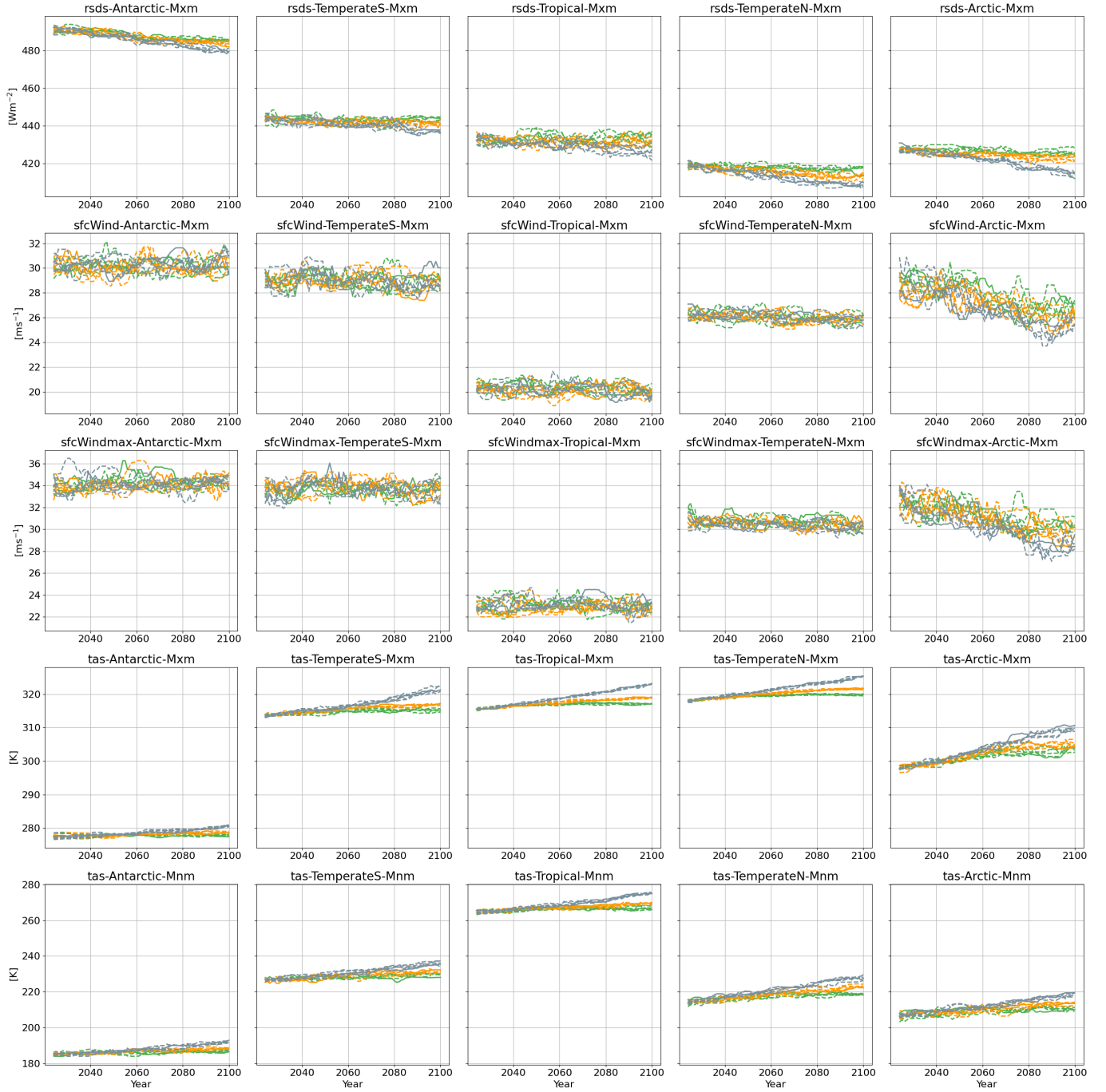Figure 2: Time-series plots of smoothed annual maximum `rsds`, `sfcWind`, `sfcWindmax` and `tas` (rows 1-4) and annual minimum `tas` (row 5), for each of 5 climate zones (columns), for `UKESM1-0-LL`. Colour indicates climate scenario (`SSP126`, green; `SSP245`, orange; `SSP585`, grey) with different line style for each ensemble member. Smoothing performed using moving 10 year median filter.

smoothing) are illustrated in Figures SM3-SM9 for each of the seven GCMs in turn, for comparison, showing generally consistent features.

Note however that `MRI-ESM2-0` (Figure SM7) offers dubious values ($\gg 100\text{ms}^{-1}$) for `sfcWindmax` in the Temperate North, considered unreasonable. For this reason, `MRI-ESM2-0` data for `sfcWindmax` is not admitted into the analysis. Note also the large growth in `sfcWind` and `sfcWindmax` under scenario `SSP126` for `EC-Earth3` in the Tropical zone (Figure SM6); these values ($\approx 35\text{ms}^{-1}$) are not unusual compared to values in other zones, and for this reason they are retained for the analysis. Note also a suspect value in `r1i1p1r1` for `NorESM2-0-LL` `tas` minimum for scenario `SSP245` in the Antarctic (and hence Global), see Figures SM1 and SM8 for illustration: we have ignored this run for analysis of annual minima, but included for analysis of means and maxima (since the offending point is of negligible influence).

Regarding the trends observed in `rsds` across climate zones, physically we know that the Antarctic typically has clearer skies, especially during the summer months, whereas the Arctic often has more persistent cloud cover. Further, during the respective summer seasons, the sun angle in the Antarctic can be slightly higher on average due to the Earth's tilt. Moreover, the Antarctic ozone hole can lead to higher UV radiation levels reaching the surface during the spring and early summer. Downward trends with time per climate zone reflect increase concentrations of aerosols. For `tas`, lower values in the Antarctic compared to the Arctic occur due to the moderating influence of oceans in the latter.

In summary, climate scenario effects on wind speed variables are less pronounced than on `rsds` and `tas`, with the exception of the Arctic zone; physically, perhaps this is related to the occurrence of polar lows and cyclonic systems there, but it not clear why these effects would also influence the Temperate North, at least to some extent.

Figures SM10-SM16 show corresponding global annual mean time-series for the seven GCMs in turn, for further comparison. Again, there is good general consistency across GCMs. However, trends across climate zones for global annual means are quite different to those for global annual maxima; e.g. compare `rsds` across climate zones in Figures SM9 and SM16. This suggests that the shape of the distribution of climate zone annual `rsds` in particular changes with climate zone.

In an attempt to summarise temporal trends and scenario trends for all GCMs and climate zones concisely, Figure 3 reports the linear trend slope found in the annual maximum data calculated for each combination of climate variable, ensemble member, climate zone and GCM, from a linear regression analysis. We omit uncertainty bars on slope estimates for clarity. Note that the figure summarises the change in value of a climate variable within a climate zone, rather than the general level of a climate variable in that zone (for which illustrations like those in Figure 2 and Figures SM3-9 are more useful). Note also that the fitting of a linear model is performed only to provide a statistic to summarise temporal trends. More suitable approaches to model fitting for annual extremes and annual means are discussed in Sections 3. Again, clearest trends with scenario are observed for `tas` and then for `rsds`, particularly in
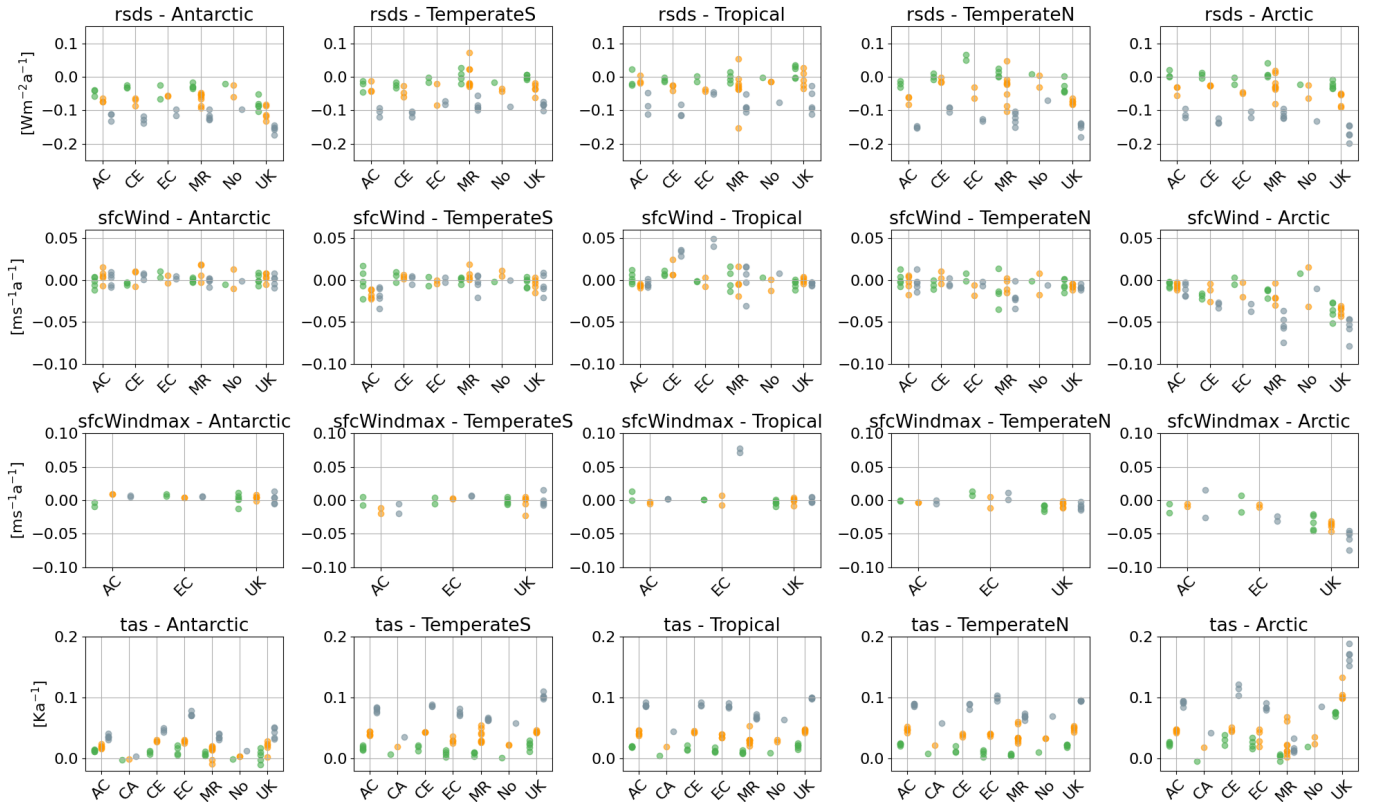

Figure 3: Slopes of linear regression lines fitted directly to the annual maximum data for each climate variable, given climate zone, GCM, climate scenario and ensemble member. Rows indicate different climate variables. Columns indicate climate zone. Discs indicate slopes for (multiple) ensemble members, and disc colour indicates climate scenario (`SSP126`, green; `SSP245`, orange; `SSP585`, grey). Units of slopes are rates of change of value per annum.

the Arctic zone. Here, for `tas` under `SSP585`, some GCMs indicate a rate of increase of temperature of $> 0.1K$ per annum; the `UKESM1-0-LL` GCM appears to produce particularly high annual rates of temperature increase. The Arctic zone also provides the clearest trends with scenario for `sfcWind` and `sfcWindmax`, with a small decrease in wind speeds

(of $\approx 0.05 \mathrm{ms}^{-1}\mathrm{a}^{-1}$) with increased climate forcing. Outside the Arctic, scenario trends in `sfcWind` and `sfcWindmax` are negligible. As noted previously, `MRI-ESM2-0` GCM output is suspect for `sfcWindmax` in the Temperate North zone and not admitted into the analysis. Corresponding linear slope estimates for climate zone minima of `tas` and climate zone means for all climate variables are summarised in Figures SM17 and SM18. Trends in `sfcWind` and `sfcWindmax` are negligible in magnitude, but again it is interesting to observe e.g. consistent downward (upwards) trends with increasing climate forcing in the Temperate North (Arctic) across GCM.

2.2. North Atlantic and Celtic Sea data

From an engineering perspective, it is interesting to examine the impact of climate change on specific locations, as well as more globally. For this reason, we also undertake statistical analysis of location-specific annual maxima of `rsds`, `sfcWind`, `sfcWindmax` and `tas` for two neighbourhoods of locations in the North Atlantic and in the vicinity of the Celtic Sea, illustrated in Figure 4. The North Atlantic neighbourhood corresponds to one of the stormiest regions on the planet, whereas the Celtic Sea neighbourhood encompasses sheltered locations in shallow water and on land. We might expect therefore that the characteristics of extreme events would be materially different in the two neighbourhoods, despite their geographic proximity. In the figure, note that GCMs use different spatial grids in
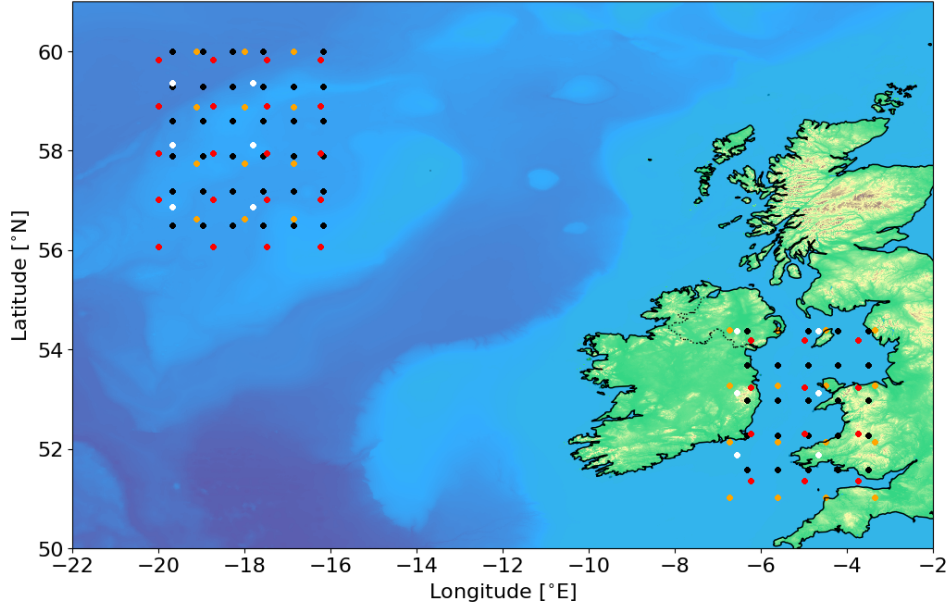

Figure 4: Discs showing grid locations of CMIP6 data accessed in the North Atlantic and the neighbourhood of the Celtic Sea. Disc colours represent climate model grids: `ACCESS-CM2` and `UKESM1-0-LL` (white), `CAMS-CSM1-0` and `MRI-ESM2-0` (orange), `CESM2` and `NorESM2-0-LL` (red), `EC-Earth3` (black). Background bathymetry-topography data accessed from GEBCO (2023); blue bathymetry palette on [-5000,0]m, and green-yellow topography palette on [0,1500]m.

general, but that some GCMs share a common grid; for the 7 GCMs considered here, in fact only 4 different spatial grids are employed, with GCM pairs `ACCESS-CM2` and `UKESM1-0-LL`, `CAMS-CSM1-0` and `MRI-ESM2-0`, and `CESM2` and `NorESM2-0-LL` using common grids.

Illustrations of time-series of annual data for centre locations of the North Atlantic and Celtic Sea neighbourhoods considered, for the four climate variables from each of the seven GCMs, and given in Figures SM19-20. For both neighbourhoods, there are no obvious temporal or scenario trends visible of variables other than `tas`. Even for `tas`, there is no consistency in trends across GCM in the North Atlantic; indeed, `MRI-ESM2-0` and `NorESM2-0-LL` suggest decreasing trends in time under scenarios `SSP126` and `SSP245`. In the Celtic Sea however, trends for `tas` across GCMs appear more similar.

3. Methodology

We consider two statistical models in the current work. The first uses generalised extreme value regression (GEVR) to estimate models for (temporal and spatio-temporal) block maxima (BM) of climate variables, and is outlined in Section 3.1. The second uses non-homogeneous Gaussian regression (NHGR) to estimate models for (temporal and spatio-temporal) means of climate variables, outlined in Section 3.2. For both GEVR and NHGR, temporal blocks

correspond to years, and spatial blocks to the whole globe or to one of five climate zones, as set out in Section 2.1. For both models, following Ewans and Jonathan (2023), we assume that all model parameters vary linearly over the period of observation, unless stated otherwise. That is, for any model parameter η, we assume that

$$\eta_t = \eta(t) = \eta^0 + \frac{t - 2015}{P - 1}\eta^1, \text{ for } t = 2015, 2016, \dots \tag{4}$$

in year t, where η^0 is the parameter value at the start year (i.e. $t = 2015$), and η^1 is the change in η over the period (2015, 2100) of length $P = 86$ years to be estimated. Further, we assume access to a sample of annual observations $\{x_i\}_{i=1}^P$ of events from X_t for analysis, for different choices of CMIP6 GCM output.

3.1. Non-stationary generalised extreme value regression

Asymptotic extreme value theory (e.g. Coles 2001, Jonathan and Ewans 2013) shows that block maxima of random draws from a max-stable distribution follow the GEV distribution for sufficiently large block length. We therefore assume that the sample $\{x_i\}_{i=1}^P$ of (temporal or spatio-temporal) BM X_t ($t = 1, 2, 3, \dots, P$) follows the GEV distribution with non-stationary location parameter $\mu_t \in \mathbb{R}$, scale $\sigma_t > 0$, shape $\xi_t \in \mathbb{R}$ and log density function

$$\log f_{\mathrm{GEVR}}(x|\mu_t, \sigma_t, \xi_t) = \begin{cases} -\left[1 + (\xi_t/\sigma_t)(x - \mu_t)\right]^{-1/\xi_t} & \xi_t \neq 0 \\ \exp(-(x - \mu_t)/\sigma_t) & \xi_t = 0. \end{cases} \tag{5}$$

Model parameters $\eta_t \in \{\mu_t, \sigma_t, \xi_t\}$ vary with t as described in Equation 4. The T-year return value Q_t for year t is estimated as the $p = 1 - 1/T$ quantile of the corresponding GEVR distribution function $F_{GEVR}(x; t)$, so that

$$Q_t = \begin{cases} (\sigma_t/\xi_t)\left[(-\log p)^{-\xi_t} - 1\right] + \mu_t & \xi_t \neq 0 \\ \mu_t - \sigma_t \log(-\log p) & \xi_t = 0. \end{cases} \tag{6}$$

Note that we only consider the case $T = 100$ years in the current work for definiteness.

Parameter estimation is performed using Bayesian inference as described in Appendix A, yielding a sample of n_I joint posterior estimates $\{\widehat{\mu}_{(k)}^0, \widehat{\mu}_{(k)}^1, \widehat{\sigma}_{(k)}^0, \widehat{\sigma}_{(k)}^1, \widehat{\xi}_{(k)}^0, \widehat{\xi}_{(k)}^1\}_{k=1}^{n_I}$ where $n_I = 10,000$. These can be used to estimate the empirical distribution of quantities of interest, such as return values Q_{2025}, Q_{2125}, and the difference

$$\Delta^Q = Q_{2125} - Q_{2025} \tag{7}$$

in return value over the 100 years from 2025 to 2125. Discussion and illustration of estimated posterior cumulative distribution functions of parameters, Q_{2025}, Q_{2125} and Δ^Q is provided in Section 4 below, in panels (a) of Figures SM21-24, and in Figure SM25. Note that extreme value analysis for annual minimum data for `tas` (over some spatial domain) is performed via characterisation of the right hand tail of the distribution of negated data.

3.2. Non-homogeneous Gaussian regression

Here we assume that the sample $\{x_i\}_{i=1}^P$ of (temporal or spatio-temporal) means X_t ($t = 1, 2, 3, \dots, P$) follows a non-homogeneous Gaussian distribution with non-stationary mean parameter $\alpha_t \in \mathbb{R}$, scale $\beta_t > 0$ and log density function

$$\log f_{\mathrm{NHGR}}(x|\alpha_t, \beta_t) = -\log\left(2\pi\beta_t^2\right)/2 - (x - \alpha_t)^2/(2\beta_t^2). \tag{8}$$

Model parameters $\eta_t \in \{\alpha_t, \beta_t\}$ again vary with t as described in Equation 4. Using the Bayesian inference scheme outlined for GEVR, we are able to estimate a chain of posterior estimates $\{\widehat{\alpha}_{(k)}^0, \widehat{\alpha}_{(k)}^1, \widehat{\beta}_{(k)}^0, \widehat{\beta}_{(k)}^1\}_{k=1}^{n_I}$ for parameters with which to estimate empirical distributions of any quantities of interest, such as the change in mean $(100/86)\alpha_1$ over any 100-year period, and specifically for the period (2025, 2125). The predicted value of X_t in year t is given by

$$M_t \sim N(\alpha_t, \beta_t^2). \tag{9}$$

Discussion and illustration of estimated posterior cumulative distribution functions of model parameters and the change

$$\Delta^M = M_{2125} - M_{2025} \tag{10}$$

in mean over the period (2025, 2125) is provided in Section 4 below and panels (b) of Figures SM21-24.

A synoptic analysis (using linear mixed effects models) and discussion of findings for variation of both Δ^Q and Δ^M with climate variable, climate scenario, climate model and its consistent ensembles is provided in Section 5 and Section SM6.

4. Results

In this section, we apply the GEVR methodology from Section 3.1 to estimate changes in 100-year return values over the period (2025,2125) for samples of spatio-temporal extremes (e.g. global or climate zone annual maxima or annual minima) for climate variables corresponding to different choices of GCM, climate scenario and ensemble member. We also apply the NHGR methodology from Section 3.2 to estimate changes in annual global and climate zone means over the same period. Inferences for global and climate zone annual means and extremes are interesting to characterise risk over large spatial scales. However, metocean design is usually performed for specific locations. For this reason we also consider GEVR inferences for annual maxima from individual locations in the neighbourhoods of the North Atlantic and Celtic Sea. As outlined in Section 3 and Appendix A, all GEVR and NHGR inferences are made using Markov chain Monte Carlo (MCMC). The section is structured as follows. In Section 4.1, we consider inferences for global maxima, means and minima. In Section 4.2, inferences for maxima, means and minima partitioned by climate zone are discussed. Finally, in Section 4.3, results for annual maxima at multiple individual locations in the North Atlantic and Celtic Sea neighbourhood are compared.

4.1. Global

Here we consider GEVR analysis of annual global maximum and minimum data, and NHGR analysis of annual global mean data, prepared from the underlying location data using the approach described in Section 2.1. We summarise results in terms of box-whisker plots for the posterior distribution of the change in 100-year return value Δ^Q, aggregated over all relevant climate ensemble members, for each climate variable over the period (2025, 2125), for different climate scenarios. Results are illustrated in Figure 5. For `rsds`, the GCMs generally indicate a small decrease in the 100-year
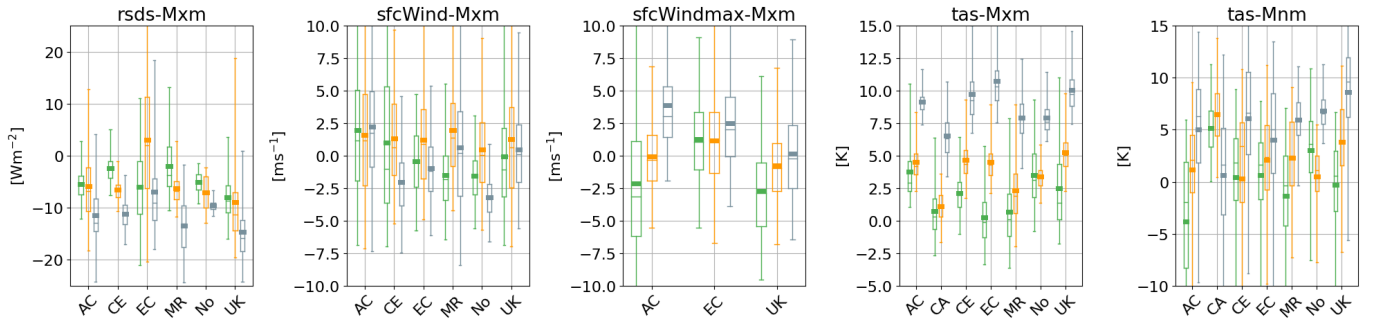

Figure 5: Box-whisker plots for the posterior distribution of the change Δ^Q in 100-year return value Q_t of global annual maximum and minima over the next 100-years, for each of `ACCESS-CM2`, `CESM2`, `EC-Earth3`, `MRI-ESM2-0`, `NorESM2-0-LL` and `UKESM1-0-LL` GCMs; the first two characters of the GCM name are used for concise labelling. Columns 1-4 correspond to change Δ^Q for global annual maxima of `rsds`, `sfcWind`, `sfcWindmax` and `tas`. Column 5 corresponds to change Δ^Q for global annual minima of `tas`; "Mxm" and "Mnm" in titles refer to maximum and minimum respectively. For each GCM, colour distinguishes climate scenarios (`SSP126`, green; `SSP245`, orange; `SSP585`, grey). For each box-whisker, the box represents the central (25%, 75%) interval for the posterior distribution, and the whisker the central (2.5%, 97.5%) interval. The posterior median is shown as a thin horizontal line (of the same width as the box), and the posterior mean as a thicker horizontal line. Vertical extents of panels have been restricted so that all central (25%, 75%) intervals are relatively clear. Relevant samples from posterior distributions for each of multiple ensembles are aggregated to estimate box-whisker structures.

return value of the global annual maximum over next 100 years. Generally, there is also some indication that Δ^Q reduces with increased climate forcing. For `sfcWind`, all central (25%, 75%) box intervals for `SSP126` and `SSP245` scenarios include zero, suggesting no strong evidence for a change in return value. For the `SSP585` scenario, the `CESM2` and `NorESM2-0-LL` GCMs in particular provide stronger evidence for a small reduction in return value of around 3ms^{-1} (but the central (2.5%, 97.5%) whisker intervals nevertheless include zero). For `sfcWindmax`, there is weak evidence for a trend of increasing change in Δ^Q with climate forcing, of the order of 5ms^{-1}. The least ambiguous inferences can be drawn for global annual maxima for `tas` in the fourth panel, which generally show an increasing trend in Δ^Q for all GCMs, with values of around 9K under scenario `SSP585`. Results for global annual minima for `tas` in the last panel are noisier, but generally similar: the figure indicates that the change in the 100-year return value for annual minimum of `tas` is generally positive with increasing climate forcing; that is, extremely low temperatures occur less often in 2125 than 2025. In summary, results for `tas` are considerably clearer than those for other climate variables. For `sfcWind` and `sfcWindmax`, of most interest for offshore and coastal design, results are somewhat contradictory: there is some evidence that return values for `sfcWind` reduce under `SSP585`, whereas there is more consistent evidence across GCMs that `sfcWindmax` increases with climate forcing.

To understand the nature of the change in the tail of the distribution of global annual maxima further, Figures 6 and 7 show estimated posterior cumulative distribution functions for the parameters of the GEVR models (see Section 3.1)
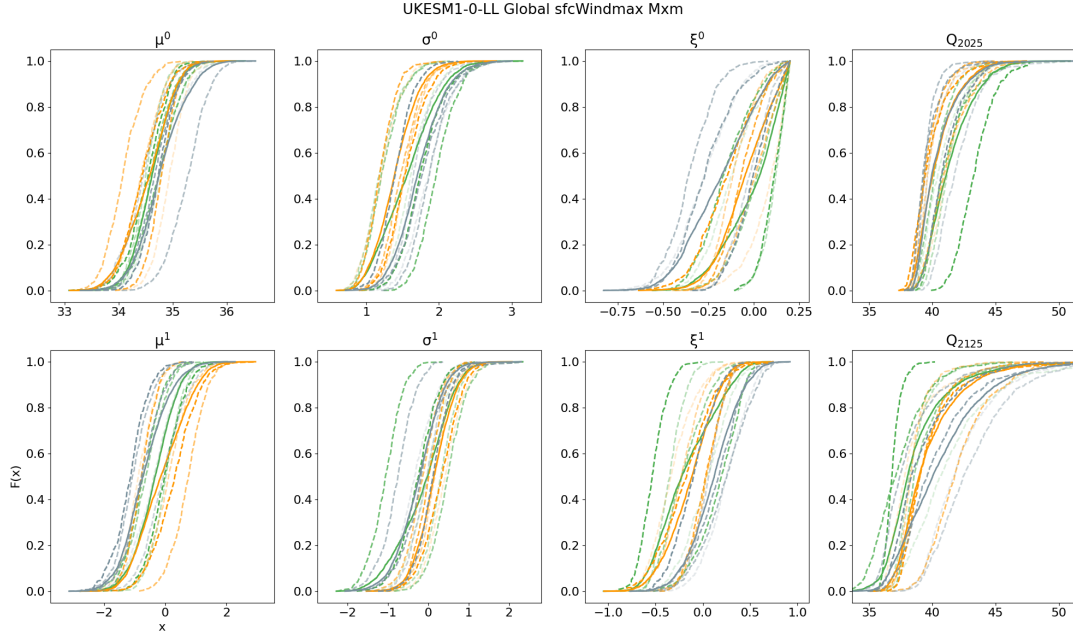
Figure 6: Estimated posterior cumulative distribution functions for GEVR model parameters and 100-year return values (Q_{2025}, Q_{2125}, for years 2025 and 2125), for the global annual maximum of `sfcWindmax` from `UKESM1-0-LL`. Colours indicate climate scenario (`SSP126`, green; `SSP245`, orange; `SSP585`, grey). Dashed line styles indicate inferences for different ensemble members; a solid line corresponds to the ensemble mean cumulative distribution function. Model parameters are the GEV location μ^0, scale σ^0 and shape ξ^0 in 2015, and the changes μ^1, σ^1 and ξ^1 in those parameters over the period (2015,2100).
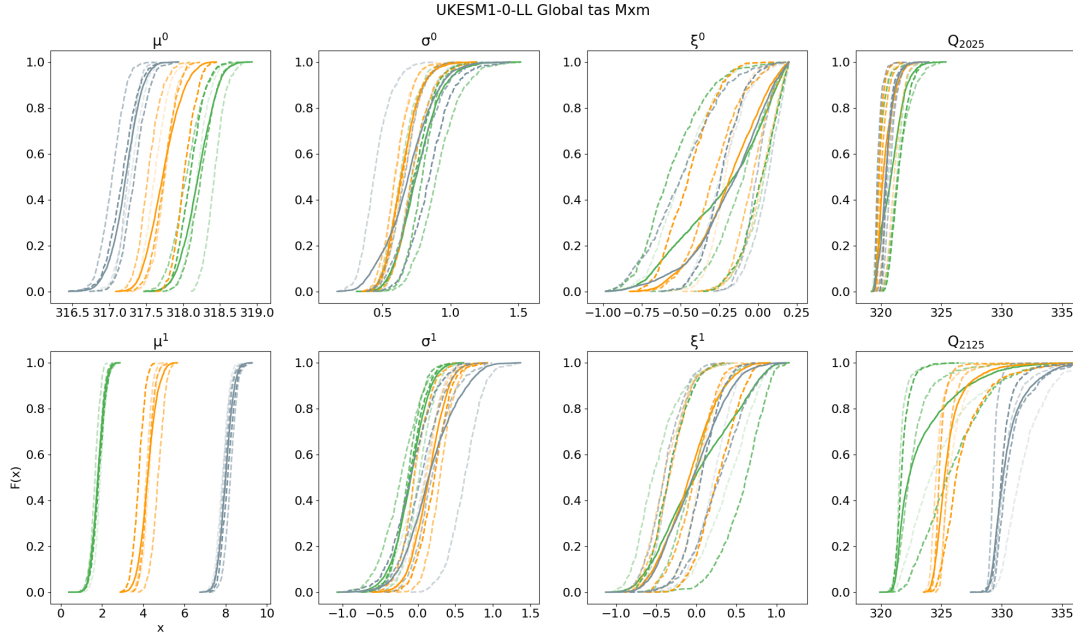

Figure 7: Estimated posterior cumulative distribution functions for GEVR model parameters and 100-year return values (Q_{2025}, Q_{2125}, for years 2025 and 2125), for the global annual maximum of `tas` from `UKESM1-0-LL`. For other details, see Figure 6.

for `sfcWindmax` and `tas` from the `UKESM1-0-LL` GCM. In Figure 6, it is difficult to discern any systematic trends between climate scenarios; indeed the variability between inferences for different ensemble members for the same scenario appears to be of the same order as that for different scenarios. In Figure 7 however, the effect of scenario on μ^1 is most obvious; this indicates a change of around 2K in the 100-year return value for global annual `tas` over the period (2015,2100) under scenario `SSP126`, rising to around 4K under `SSP245` and 8K under `SSP585`. That is, changes in the general level of `tas` lead to clear differences in Q_{2125} shown in the bottom right panel. In contrast, there is

considerably less evidence for clustering with respect to scenario for variables σ and ξ, responsible for the shape of the distributional tail. That is, there is little evidence in the data that the shape of the distributional tail changes in time. We also note a change in μ^0 (the value of GEV "level" in 2015, with posterior medians varying by around 1K from around 317.2k to 318.2K under the different scenarios) which provides a minor counter-effect for the change in μ^1.

Figure 8 summarises the change Δ^M in the global mean of each of the four climate variables over the next 100 years. Results reflect data characteristics mentioned in Section 2. For `rsds`, there is agreement across GCMs that increased climate forcing will reduce mean value. Findings for `tas` are consistent across GCM. Relative to the size of change indicated by `tas`, changes in global mean `sfcWind` and `sfcWindmax` are very small ($\ll 1\mathrm{ms}^{-1}$ in magnitude), with some evidence for minor climate scenario effect.
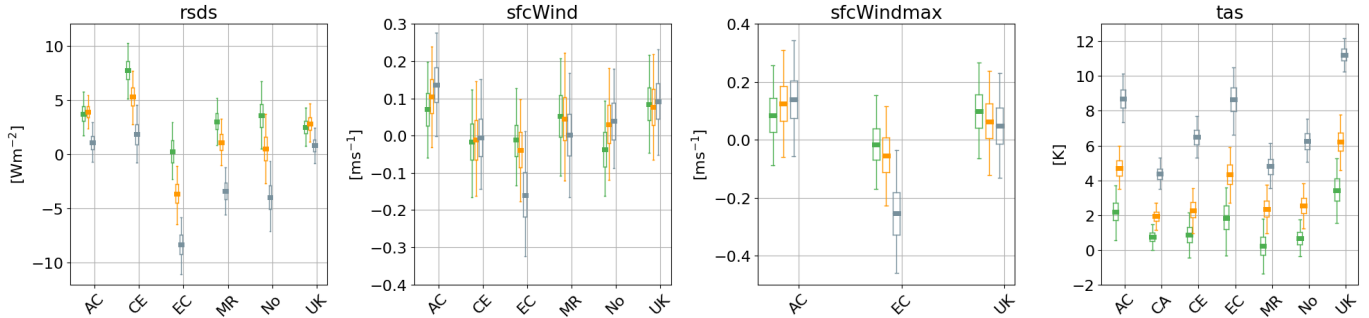

Figure 8: Box-whisker plots for the change Δ^M in global mean over the next 100-years, for each of the four climate variables. For details, see Figure 5.

Supporting Figures SM21-24 (panels (b)) provide estimated posterior cumulative distribution functions for parameters of NHGR models for all four climate variables from `UKESM1-0-LL` GCM; panels (a) of the same figures report the corresponding estimates for GEVR parameters. The most obvious feature of these figures for GEVR models of global annual maxima and minima, is again evidence for a scenario-related change in level μ^1 (rather than for tail parameters σ^1 and ξ^1), for `rsds` and `tas`. For NHGR models of global mean data, evidence for scenario-related change in level α^1 is present for both `rsds` and `tas`. For the latter, there is also evidence for change in standard deviation β^1. Smaller competing changes in α^0 and β^0 are present, particular for `tas`, suggesting that the modelling assumption of a linear trend in NHGR parameters with time may not always be reasonable for `tas`.

4.2. Climate zones

Physical intuition, together with the exploratory analysis in Section 2, suggests that there may be considerable variation in changes Δ^Q and Δ^M across climate zones. For this reason, we extend the GEVR analysis of global annual extremes and NHGR analysis of global annual means to the corresponding climate zone annual extremes and means, for the Antarctic, Temperate South, Tropical, Temperate North and Arctic climate zones (see Section 2.1). Results of the analysis are summarised in Figure 9 in terms of the change Δ^Q in 100-year return value, and Figure 10 in terms of the change Δ^M in mean for NHGR.

Results in Figure 9 are generally similar to those for global annual extremes in Figure 5. The estimated posterior distributions for Δ^Q are wider that the corresponding global estimates, possibly due to the reduction in size of spatial domain over which annual maxima are taken per climate zone. For `sfcWind` and `sfcWindmax`, the central (25%,75%) box region typically includes zero for all combinations of GCM and climate scenario, indicating no obvious change in 100-year return values over the next 100 years for all climate zones, with the exception of the Arctic: here, there is weak evidence for more negative Δ^Q under `SSP585`. For `rsds`, there is general evidence for reduction of Δ^Q with increased forcing. For annual maxima and minima of climate zone `tas`, there is strong evidence for a scenario effect, with the `UKESM1-0-LL` GCM suggesting considerably more Arctic heating than other models and other climate zones. There is also surprisingly consistent evidence across GCMs for large $\Delta^Q \approx 20$K for `tas` minima in the Temperate North under `SSP585`. The anomalous behaviour of some estimates in Figure 9 (e.g. for `sfcWindmax` from `EC-Earth3` in the tropics under `SSP585`) is to be expected given similar anomalous behaviour in the underlying climate zone annual maximum data (e.g. Figure SM6 for `sfcWindmax` in the tropics).

Corresponding estimates for change Δ^M in the climate zone annual mean values are given in Figure 10. Here, it is noticeable that trends with scenario are clearer across GCM than for changes in 100-year return value; this is due in part at least to the relative efficiency of estimating sample means rather than sample tails. However, the trends also appear to be more consistent across GCM. The exaggerated extent of changes in the Arctic climate zone is also clear, presumably related to a reduction in the extent of surface ice. Visually at least, partitioning the globe into climate
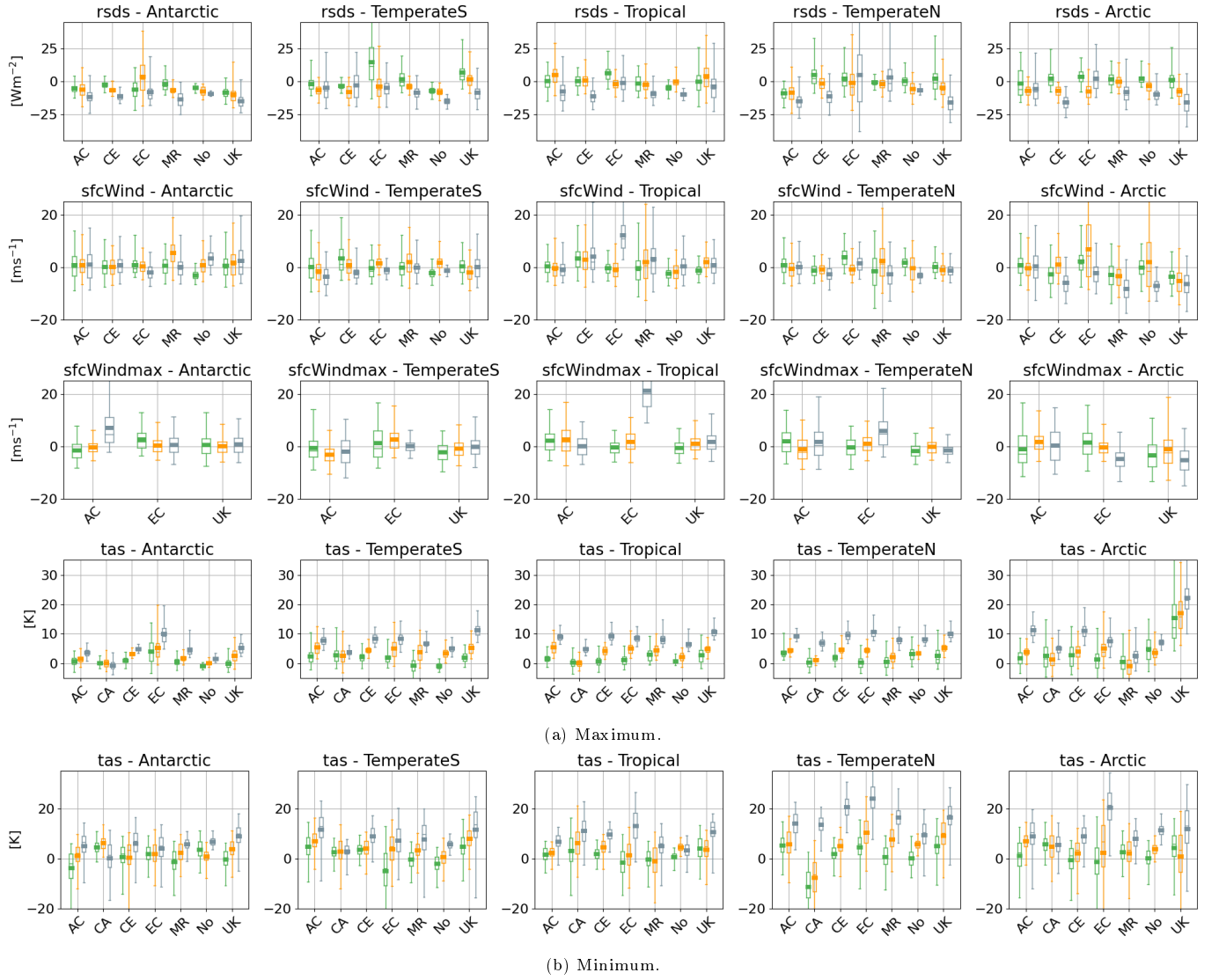
(a) Maximum.

(b) Minimum.

Figure 9: Box-whisker plots for the estimated posterior distribution of the change Δ^Q in (a) the 100-year return value of the climate zone annual maximum, and (b) the 100-year return value of the climate zone annual minimum for `tas`. Columns provide results for the Antarctic, Temperate South, Tropical, Temperate North and Arctic climate zones. For other details, see Figure 5. Results from analysis of one ensemble member for global minima of `NorESM2-0-LL tas` under scenario `SSP245` omitted; see notes in Section 2.1.

zones appears to improve the consistency of trends with scenario across GCMs for `rsds`. In the Antarctic, there is evidence for a reduction in annual mean `rsds` under all scenarios, with the amplitude of reduction increasing with climate forcing. The climate scenario effect is strongest in the Arctic. For `sfcWind` and `sfcWindmax`, changes in mean climate zone values are small with magnitudes $\ll 1\mathrm{ms}^{-1}$ everywhere except the Arctic. In the Arctic, a number of GCMs suggest that the annual mean for both `sfcWind` and `sfcWindmax` will increase with climate forcing. For `tas`, we again see consistent trends across GCMs, with largest effects of climate forcing amounting the changes Δ^M of around 10K in the Arctic.

It is interesting that in general changes Δ^Q reflect changes Δ^M. That is, in broad terms, change in 100-year return value over the next 100 years is largely driven by change in the general level of the climate variable, rather than change to the shape of the tail of the distribution of the climate variable; a similar observation was made in Section 4.1 regarding the importance of μ^1 in the analysis of global annual maxima.
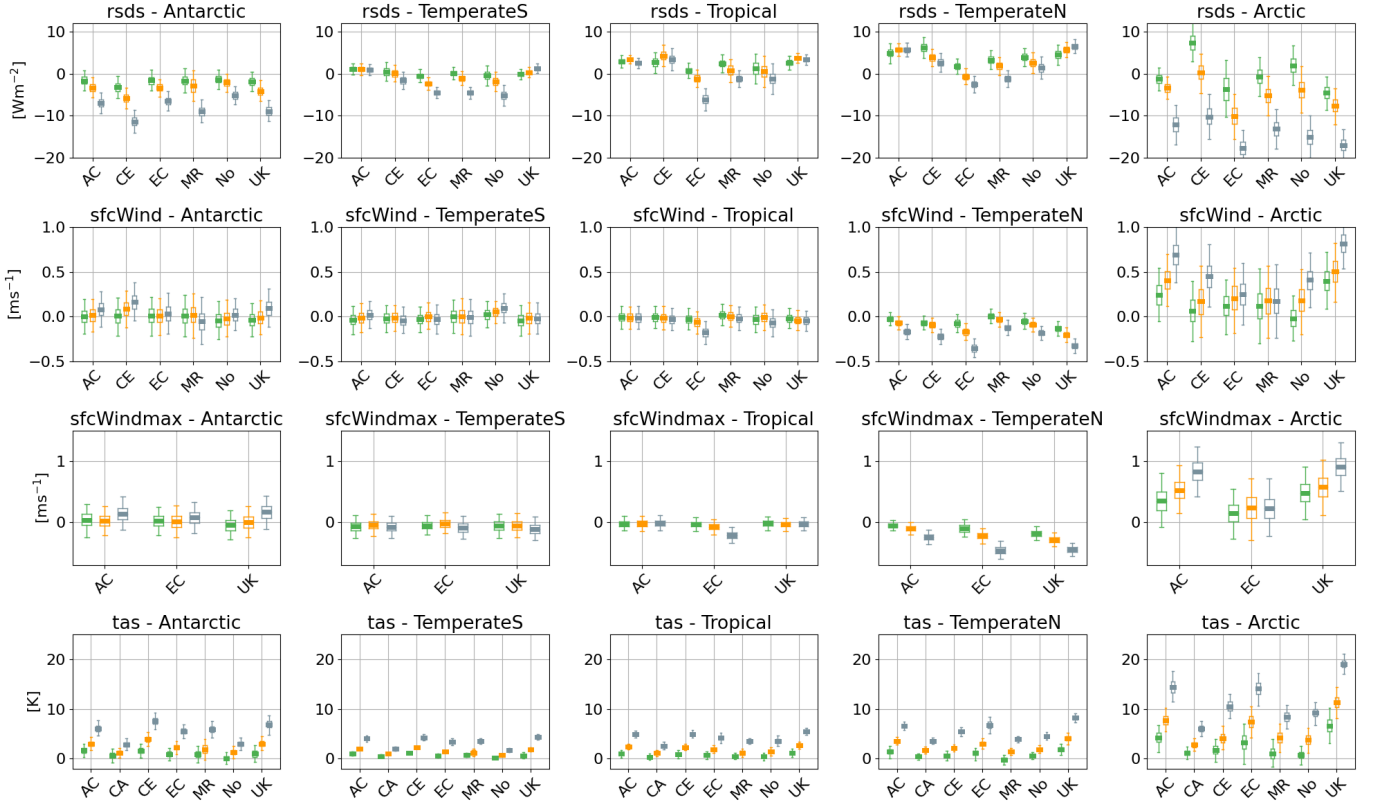
12

Figure 10: Box-whisker plots for the change Δ^M in the climate zone annual mean value over the next 100-years. Rows indicate different climate variables. Columns indicate climate zone. For other details, see Figure 5.

4.3. North Atlantic and Celtic Sea

For annual maximum data from locations in the North Atlantic and Celtic Sea neighbourhoods, we estimate the posterior distribution of the change Δ^Q in 100-year return value over the next 100-years independently for each combination of location, GCM, climate variable, scenario and ensemble member. For conciseness of presentation, we then aggregate estimates for the posterior distribution of Δ^Q over location (within neighbourhood) and climate ensemble, resulting in distributional estimates for Δ^Q from each combination of climate variable, GCM, geographic neighbourhood and climate scenario. These are summarised in Figure 11 in terms of box-whisker plots. Inspection of the figure suggests that changes Δ^Q in rsds are somewhat more positive in the North Atlantic compared with the Celtic Sea neighbourhood, although the central (25%,75%) box region often includes zero, indicating little evidence for a change in 100-year return value. There is also some evidence for reduction of rsds with increased forcing, particularly for the Celtic Sea neighbourhood; a reduction by as much as $10\mathrm{Wm}^{-2}$ is suggested under scenario SSP585. There are no trends at all of interest for sfcWind and sfcWindmax, with almost all central (25%,75%) box regions including zero. There is evidence for increasing tas with climate forcing in both the North Atlantic and Celtic Sea neigbourhoods, and that changes in the Celtic Sea neighbourhood are likely to be somewhat larger than in the North Atlantic.
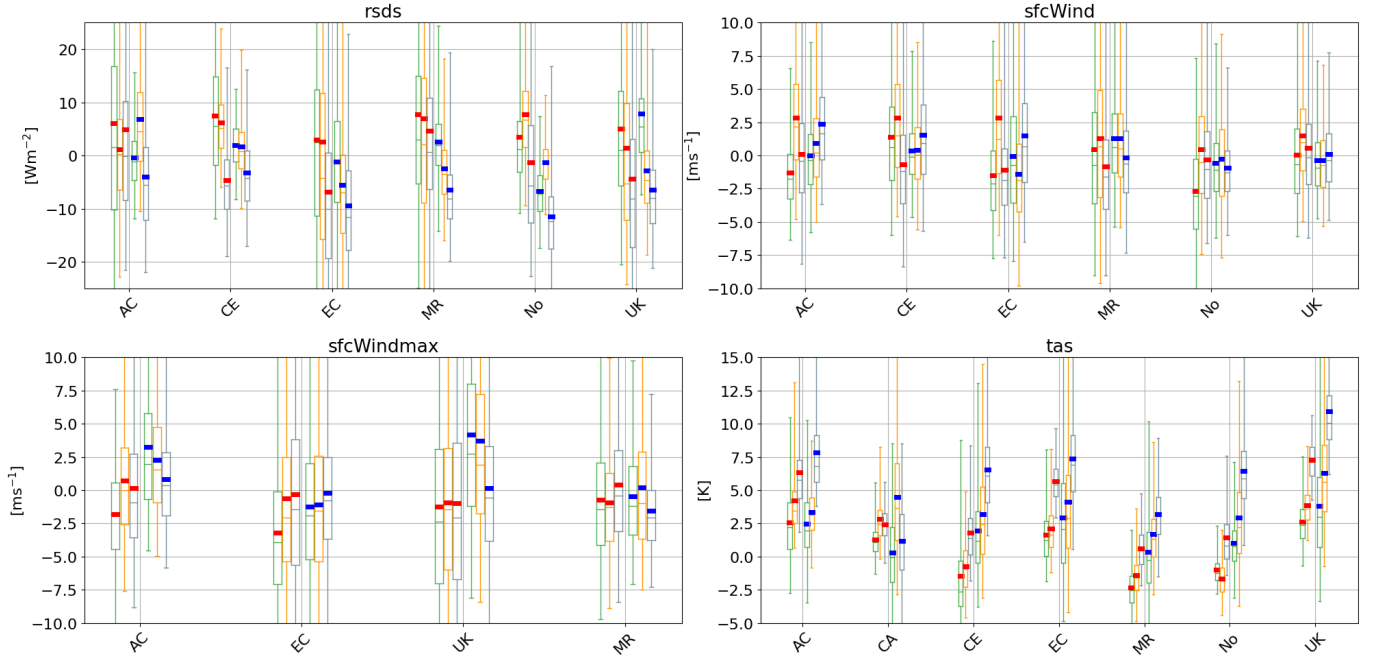
Figure 11: Box-whisker plots for the change Δ^Q in 100-year return values over the next 100-years for the North Atlantic and Celtic Sea neighbourhoods. Panels show results for different climate variables. Within each panel, inferences per climate model are given as a cluster of 6 box-whiskers: left-hand box-whiskers (with means in red) for the North Atlantic and right-hand (with means in blue) for the Celtic Sea. Box-whisker outline colour indicates climate scenario (`SSP126`, green; `SSP245`, orange; `SSP585`, grey).

5. Discussion and conclusions

There is a wealth of evidence that climate change is occurring (IPCC 2013, IPCC 2021). It is pertinent therefore to assess what evidence is present in output of the latest climate models for changing characteristics of extremes of wind, surface solar irradiance and temperature.

We estimate global and climate zone annual maximum and annual mean data for four climate variables (`sfcWind`, `sfcWindmax`, `rsds` and `tas`) and annual minimum also for `tas`, for the period (2015,2100) from output of seven CMIP6 GCMs. We also calculate the corresponding annual data for neighbourhoods of locations in the North Atlantic and the Celtic Sea region. For each data source we access output corresponding to three climate scenarios and multiple climate ensemble runs. We then estimate non-stationary extreme value models (GEVR) for annual extremes, and perform non-homogeneous Gaussian regression (NHGR) for annual means. Using the estimated statistical models, we further estimate (i) the change Δ^Q in the 100-year return value for annual extremes, and (ii) the change Δ^M in the annual mean level over the period (2025, 2125).

Inspection of results from Section 4 reveals inconsistencies in estimates of Δ^Q and Δ^M across GCMs, but in general we can draw the following conclusions. Unsurprisingly, but importantly, inference for mean trends is more efficient than for extreme quantiles. That is, it is easier to identify trends in means than in extreme quantiles with confidence. For climate zone annual means, there is evidence for small changes in Δ^M for wind variables as a function of climate scenario, but the direction of these changes differs by GCM and climate zone. For extremes of wind variables, the estimated posterior distribution of Δ^Q is considerably broader and centred near zero; there is no consistent evidence for change in return value (except perhaps in the Arctic zone), and changes in posterior mean of around $\pm$ 5ms^{-1} are typical across GCMs. In contrast, estimated changes for `rsds` and `tas` are considerably more convincing. For `rsds` there is clear evidence for a reduction in mean of around 10Wm^{-2} when comparing `SSP585` with `SSP126` in the Antarctic, and even larger reductions in Arctic. There is some evidence for reduction in Δ^Q for climate zone annual maxima with increased climate forcing. For `tas` there is clear evidence for increase in global and climate zone annual means, maxima and minima with increased forcing. Inspection of estimated posterior distributions of extreme value model parameters reveals that changes in Δ^Q for `rsds` and `tas` can be explained by a change in level μ^1 rather than changes in the tail characteristics of the distribution of climate variable quantified by σ^1 and ξ^1 in the GEVR model. For single location analysis of annual maxima in the North Atlantic and Celtic Sea region, uncertainties in inferences for Δ^Q are large. Hence it is difficult to be confident about the presence of climate change effects even for changes in the 100-year return values of wind variables and `rsds`; systematic climate effects in `tas` are nevertheless present.

14

5.1. Expected changes in return value, and probability of return value increase

It is important to consider the practical implications of the findings of this work, particularly for changes in the 100-year return value of the annual maximum over the next 100 years of wind variables. Despite the large variability of inferences for Δ^Q for wind variables, if we are prepared to assume that all GCMs are equally informative, we can estimate the expected change Δ^Q in return value for each of the climate variables empirically, simply by aggregating the samples of estimates for the return value differences from Section 4. We can also estimate the probability that an increase in return value will occur. Results per climate zone and scenario are given in Table 2. Empirical probabilities

Variable	Zone	$\mathbb{E}(\Delta^Q)$			$\mathbb{P}(\Delta^Q > 0)$		
		$SSP126$	$SSP245$	$SSP585$	$SSP126$	$SSP245$	$SSP585$
rsds [Wm^{-2}]	GL	-4.89	-6.06	-12.15	0.15	0.13	0.04
	AN	-4.93	-6.02	-12.54	0.14	0.12	0.04
	TS	2.78	-2.54	-6.46	0.49	0.27	0.18
	TR	0.24	2.37	-6.12	0.51	0.49	0.21
	TN	0.09	-3.62	-7.47	0.41	0.27	0.21
	AR	1.46	-4.51	-9.18	0.52	0.2	0.18
sfcWind [ms^{-1}]	GL	0.21	1.41	0.23	0.42	0.58	0.47
	AN	0.45	1.85	1.21	0.47	0.59	0.51
	TS	0.55	0.05	-1.16	0.47	0.48	0.32
	TR	0.1	0.98	2.05	0.44	0.53	0.54
	TN	0.28	-0.08	-1.25	0.5	0.4	0.32
	AR	-1.4	-0.97	-4.64	0.36	0.35	0.19
sfcWindmax [ms^{-1}]	GL	-1.71	-0.16	1.52	0.33	0.44	0.63
	AN	0.68	0.15	2.19	0.52	0.47	0.6
	TS	-1.05	-0.46	-0.39	0.34	0.41	0.43
	TR	0.14	1.67	5.83	0.45	0.62	0.69
	TN	-0.5	-0.02	0.96	0.39	0.46	0.42
	AR	-1.68	-0.21	-3.75	0.36	0.43	0.23
tas [K]	GL	2.0	4.1	9.32	0.75	0.97	1.0
	AN	1.05	2.26	5.07	0.63	0.83	0.97
	TS	1.52	4.24	8.2	0.75	0.93	1.0
	TR	1.81	4.1	8.83	0.8	0.95	1.0
	TN	1.9	4.05	9.2	0.73	0.96	1.0
	AR	4.75	5.75	10.62	0.72	0.84	0.95

Table 2: Estimated expected change $\mathbb{E}(\Delta^Q)$ and probability of increase $\mathbb{P}(\Delta^Q > 0)$ of 100-year return values over the period (2025,2125) for annual maxima of four climate variables over 6 climate zones (GL: global; AN: Antarctic; TS: Temperate South; TR: Tropical; TN: Temperate North; AR: Arctic). Columns under "$\mathbb{E}(\Delta^Q)$" show expected changes per scenario, in the units of the variable; thus we estimate a reduction in 4.64ms^{-1} in the return value for sfcWind under scenario SSP585 in the Arctic. Columns under "$\mathbb{P}(\Delta^Q > 0)$" show corresponding probabilities of increasing return value. Estimates are calculated assuming equal weighting for each climate model. Note that the first (year 2015) observation for rsds in all CESM2 runs is spurious and has been omitted. Multiple values for sfcWindmax from MRI-ESM2-0 are also suspect (with some values > 100 ms^{-1}; see Figure SM7); for this reason MRI-ESM2-0 output is ignored for variable sfcWindmax only.

$\mathbb{P}(\Delta^Q > 0)$ near zero or unity are indicative of agreement between climate models (and their constituent ensembles) regarding a change in $\Delta^Q = Q_{2125} - Q_{2025}$. For sfcWind and sfcWindmax, we therefore see that only in the Arctic under scenario SSP585 is there evidence of agreement between models regarding a change in return value: specifically, values of $\mathbb{P}(\Delta^Q > 0) \notin (0.25, 0.75)$ are observed only in the Arctic zone under scenario SSP585. Here, mean reductions of $\Delta^Q \approx 4$ms^{-1} are estimated for sfcWind and sfcWindmax. For comparison, rsds shows significant reduction in the Antarctic and hence globally under SSP585; there is also a consistent pattern of larger reductions in polar zones than elsewhere under both SSP245 and SSP585. For tas, $\mathbb{P}(\Delta^Q > 0)$ is near unity under SSP245 and SSP585 for all climate zones.

The ocean engineer is typically interested not in summary statistics for large spatial regions such as climate zones, but rather in analysis for specific locations. To illustration the latter, Table 3 provides estimates for the expected change Δ^Q, and the probability that Q_{2125} exceeds Q_{2025}, for the central locations of the North Atlantic and Celtic Sea regions in Figure 4. Relative to the probability estimates in Table 2, probabilities in Table 3 for sfcWind, sfcWindmax and

Variable	Zone	$\mathbb{E}(\Delta^Q)$			$\mathbb{P}(\Delta^Q > 0)$		
		126	245	585	126	245	585
rsds [Wm^{-2}]	NA	12.58	6.83	-6.93	0.74	0.59	0.26
	CS	0.76	-1.15	-7.77	0.53	0.27	0.16
sfcWind [ms^{-1}]	NA	-0.73	1.68	-0.12	0.24	0.57	0.52
	CS	1.98	0.3	1.42	0.52	0.38	0.62
sfcWindmax [ms^{-1}]	NA	-2.8	-0.01	0.94	0.36	0.44	0.57
	CS	2.83	2.7	1.67	0.64	0.53	0.43
tas [K]	NA	2.14	2.18	4.06	0.68	0.67	0.96
	CS	1.92	4.43	5.95	0.68	0.89	0.92

Table 3: Estimated expected change $\mathbb{E}(\Delta^Q)$ and probability of increase $\mathbb{P}(\Delta^Q > 0)$ of 100-year return values over the period (2025,2125) for annual maxima of four climate variables at the central locations of the North Atlantic (NA) and Celtic Sea (CS) neighbourhoods. For further description, see Table 2.

rsds are nearer 0.5 than zero or unity. Moreover, the expected values Δ^Q are small in magnitude. For comparison, there is evidence under SSP585 that climate models agree on an increasing tas for both North Atlantic and Celtic Sea regions. Clear trends are present with climate scenario for both rsds and tas, but not for sfcWind and sfcWindmax.

Table SM1 of the SM estimates $\mathbb{E}(\Delta^Q)$ and $\mathbb{P}(\Delta^Q > 0)$ for change Δ^Q in annual tas minima from global and climate zones, quantifying the information already visualised in Figure 9(b). Similarly, Table SM3 quantifies $\mathbb{E}(\Delta^M)$ and $\mathbb{P}(\Delta^M > 0)$ for change $\Delta^M = M_{2125} - M_{2025}$ in the annual means for global and climate zones, showing clear trends with climate zone and climate scenario, already visualised in Figure 10.

5.2. Quantifying the effect of climate scenario, and uncertainty due to climate model and ensemble member on Δ^Q and Δ^M

We can summarise sources of variability in our data for changes in 100-year return values Δ^Q and annual means Δ^M more precisely by estimating another statistical model. Here we estimate a linear mixed effects model (LMM, e.g. West et al. 2022) using Δ^Q (or Δ^M) as a response, with climate scenarios as so-called *fixed effects*, and climate models and nested climate ensemble members (for a given model) as *random effects*. The advantage of this approach over linear regression (for all of scenario, model and ensemble) is that we assume that the climate model and ensemble output available to us are drawn randomly from large families of models and their ensemble members. We can therefore estimate the variability in Δ^Q (or Δ^M) which can be attributed to our random choices of climate model and their ensemble members; that is, we can estimate how much of the variability in Δ^Q (or Δ^M) is due to (apparently) random effects from different climate models, and from different ensemble members for a given climate model.

Using estimates of $\Delta \in (\Delta^Q, \Delta^M)$ for a given climate variable in a given climate zone, we can express the linear mixed effects model as

$$\Delta_{ijk\ell} = \iota + \gamma_j + \delta_k + \zeta_{k(\ell)} + \epsilon_{ijk\ell} \tag{11}$$

where $\Delta_{ijk\ell} \in \mathbb{R}$ is the ith observation of Δ from the extreme value model output, for climate scenario j ($j = 1, 2, 3$, corresponding to scenarios SSP126, SSP245 and SSP585), for climate model k ($k = 1, 2, ...$) and ensemble member ℓ ($\ell = 1, 2, ...$) of model k. Parameter $\iota \in \mathbb{R}$ is the intercept. Parameter $\gamma_j \in \mathbb{R}$ represents the fixed effect of scenario j on response. Parameter $\delta_k \in \mathbb{R}$ represents the random effect of climate model k on response, and $\zeta_{k(\ell)} \in \mathbb{R}$ the nested random effect of climate ensemble member ℓ for model k. Parameters $\epsilon_{ijk\ell} \in \mathbb{R}$ are model error terms. For fitting, we assume that each of δ_k, $\zeta_{k(\ell)}$ and $\epsilon_{ijk\ell}$ are independently normally-distributed with zero means and variances $\tau_\delta^2 \geq 0$, $\tau_\zeta^2 \geq 0$ and $\tau_\epsilon^2 \geq 0$. The objective of the analysis is to estimate the set $\{\gamma_j\}_{j=1}^3$ of fixed effects, the variances τ_δ^2 and τ_ζ^2 of random effects, and the error variance τ_ϵ^2. Inference was performed using algorithms from the MATLAB Statistics toolbox and checked using equivalent functionality in Julia, with scenario SSP126 ($j = 1$) as reference category for the fixed climate scenario effect. That is, to avoid issues of multicollinearity, we actually undertake estimation of the sum $\iota + \gamma_1$, together with that of scenario difference effects $\gamma_2 - \gamma_1$ and $\gamma_3 - \gamma_1$.

Results for analysis of change Δ^Q in the 100-year return value annual maxima per climate variable and zone are given in Table 4. For `sfcWind` and `sfcWindmax`, R^2_{ME} values for the full mixed effect model are < 0.3 (except for `sfcWind` in

Variable	Zone	SSP effect			Model standard deviations					R^2	
		$\iota + \gamma_1$	$\gamma_2 - \gamma_1$	$\gamma_3 - \gamma_1$	τ_R	τ_{FE}	τ_ϵ	τ_δ	τ_ζ	R^2_{FE}	R^2_{ME}
rsds $[\mathrm{Wm}^{-2}]$	GL	-4.47	-1.27	-7.26	7.62	6.93	6.25	1.56	2.51	0.17	0.33
	AN	-4.62	-1.38	-7.29	7.6	6.85	6.12	1.48	2.76	0.19	0.35
	TS	3.83	-6.43	-9.61	10.29	9.62	8.32	1.36	5.1	0.12	0.35
	TR	1.6	1.25	-7.02	10.92	10.3	9.16	0.0	6.43	0.11	0.3
	TN	0.22	-3.91	-7.95	12.06	11.68	10.17	3.04	4.69	0.06	0.29
	AR	2.44	-6.83	-11.48	10.23	9.34	8.22	2.48	4.19	0.17	0.35
sfcWind $[\mathrm{ms}^{-1}]$	GL	0.25	1.16	0.02	4.73	4.7	4.31	0.0	1.84	0.01	0.17
	AN	0.59	1.4	0.62	5.34	5.31	4.95	0.0	1.94	0.01	0.14
	TS	0.73	-0.58	-1.81	4.8	4.74	4.38	0.45	1.76	0.02	0.17
	TR	-0.58	1.06	2.48	6.1	6.05	5.5	0.0	3.13	0.02	0.19
	TN	0.38	-0.57	-1.43	4.74	4.69	4.46	0.0	1.65	0.02	0.11
	AR	-0.44	-0.17	-3.16	6.83	6.63	5.6	2.45	3.28	0.06	0.33
sfcWindmax $[\mathrm{ms}^{-1}]$	GL	-1.5	1.55	3.23	4.31	4.1	3.71	0.76	1.58	0.09	0.26
	AN	0.68	-0.53	1.51	4.94	4.87	4.54	0.0	1.74	0.03	0.15
	TS	-1.05	0.6	0.66	4.93	4.92	4.57	0.0	1.83	0.0	0.14
	TR	0.96	1.53	5.69	7.11	6.69	6.05	2.91	1.07	0.11	0.28
	TN	-0.33	0.47	1.45	4.74	4.71	4.12	0.73	2.16	0.02	0.25
	AR	-1.68	1.47	-2.11	6.72	6.56	5.65	0.0	3.35	0.05	0.29
tas $[\mathrm{K}]$	GL	1.78	2.12	7.33	3.93	2.46	2.17	0.86	0.82	0.61	0.69
	AN	0.54	1.52	4.11	3.53	3.13	2.27	1.73	1.57	0.22	0.59
	TS	1.06	3.22	6.74	3.97	2.94	2.46	1.17	1.22	0.45	0.62
	TR	1.09	2.79	7.13	3.76	2.46	2.04	1.04	1.3	0.57	0.7
	TN	1.8	2.19	7.4	3.91	2.52	2.23	0.68	0.95	0.59	0.68
	AR	4.01	1.31	6.27	8.2	7.8	4.82	4.83	3.05	0.09	0.65

Table 4: Summary of linear mixed effects modelling for the change Δ^Q in the 100-year return value of annual maxima for four climate variables over 6 climate zones (GL: global; AN: Antarctic; TS: Temperate South; TR: Tropical; TN: Temperate North; AR: Arctic). Columns under "SSP effect" show intercept ι and fixed effect parameter estimates γ_j for the change in 100-year return value of the given variable over the period (2025,2125) under scenario j, in the units of the variable; thus we estimate a reduction in $3.16\mathrm{ms}^{-1}$ in the return value for `sfcWind` under scenario `SSP585`. Columns under "Model standard deviations" provide estimates of the various standard deviations of model fitting. τ_R: the (full unconditional) standard deviation of the response R; τ_{FE}: the model error standard deviation after fitting only the fixed effects (FE, of climate scenario); τ_ϵ: the model error standard deviation after fitting the full mixed effects model. τ_δ: standard deviation of climate model random effect; τ_ζ: standard deviation due to nested random effect of climate ensemble within climate model. R^2 statistics are also provided, from fitting only the fixed effects (FE), and from fitting the full mixed effects (ME) model. Note that the first (year 2015) observation for `rsds` in all CESM2 runs is spurious and has been omitted. See also notes about suspect values for `sfcWindmax` under model `MRI-ESM-0` in the caption of Table 2. Further, since sample size for model fitting is huge, estimates of uncertainties and "significance" are of little practical value, and are omitted.

the Arctic), and R^2_{ME} values are lower than those for `rsds` and (in particular) `tas`. This indicates that the variation in Δ^Q explainable by the effects of scenario, model and ensemble is relatively small for `sfcWind` and `sfcWindmax`. The same feature can be seen by comparing the reduction in standard deviation (from τ_R to τ_ϵ) from fitting the full mixed effects model for different variables; the reduction is generally rather modest for `sfcWind` and `sfcWindmax`. Of course this also results in relative large values of error standard deviation τ_ϵ for wind variables. Values of R^2_{FE} indicate the quality of model fit using fixed scenario effects only. For `sfcWind` and `sfcWindmax`, $R^2_{\mathrm{FE}} \approx 0$, indicating that scenario has little skill in explaining variation of Δ^Q of wind variables; it is instructive again to compare these R^2_{FE} values with those for `rsds` and `tas`. Further, we see that values of τ_ζ are relatively large for wind variables, indicating large variability between estimates of Δ^Q from ensemble members; values of τ_ζ for wind variables tend to be larger than those of τ_δ, indicating that the effect of variability between ensembles is (much) larger than that of variability between

climate models. This feature is illustrated in Figures SM28-31, showing box-whisker plots of the posterior distribution of Δ^Q for individual ensemble members, per climate variable and spatial zone. For `sfcWind` in the Temperate North e.g., variation in Δ^Q is dominated by ensemble effects, and the variation between climate models is small (leading to estimated $\tau_\delta = 0$); for `sfcWind` in the Arctic in contrast, variation between climate models is relatively large (leading to estimated $\tau_\delta \approx \tau_\zeta$). Note in comparison that the values of τ_δ and τ_ζ are also of similar magnitudes for `rsds` and `tas`; for the latter, these are also of similar magnitude to τ_ϵ. The Arctic, exhibiting an interestingly large climate model random effect for `tas`, is an exception.

Corresponding results for single location analyses of annual maxima from the centre points of the North Atlantic and Celtic Sea region are given in Table 5. Unsurprisingly, we see that the estimates for fixed scenario effects γ_j ($j = 1, 2, 3$) in Tables 4 and 5 are similar in sign and general magnitude to the expected changes $\mathbb{E}(\Delta^Q)$ estimated in Tables 2 and 3. R^2_{FE} values in Table 5 indicate that fixed scenario effects are poorer in explaining variation in return

Variable	Zone	SSP effect			Model standard deviations					R^2	
		$\iota + \gamma_1$	$\gamma_2 - \gamma_1$	$\gamma_3 - \gamma_1$	τ_R	τ_{FE}	τ_ϵ	τ_δ	τ_ζ	R^2_{FE}	R^2_{ME}
`rsds`	NA	7.86	-3.9	-10.44	22.55	22.17	20.44	0.0	8.8	0.03	0.18
$[\mathrm{Wm}^{-2}]$	CS	1.35	-3.13	-7.23	10.88	10.49	9.1	2.46	4.81	0.07	0.3
`sfcWind`	NA	-0.61	2.25	-0.08	5.08	4.98	4.48	1.26	1.95	0.04	0.22
$[\mathrm{ms}^{-1}]$	CS	0.91	-0.64	0.5	4.33	4.29	4.11	0.0	1.51	0.02	0.1
`sfcWindmax`	NA	-1.67	0.79	2.22	6.83	6.77	6.24	0.0	3.11	0.02	0.17
$[\mathrm{ms}^{-1}]$	CS	2.76	0.64	-4.23	8.09	7.85	6.97	2.67	2.87	0.06	0.26
`tas`	NA	0.46	0.89	3.29	3.61	3.33	2.21	2.05	1.18	0.15	0.62
$[\mathrm{K}]$	CS	1.72	1.84	4.42	4.35	3.96	3.46	1.26	1.45	0.17	0.36

Table 5: Summary of linear mixed effects modelling for the change Δ^Q in the 100-year return value of annual maxima for four climate variables at the central locations of the North Atlantic (NA) and Celtic Sea (CS) neighbourhoods. For further description, see Table 4.

value differences Δ^Q for the central locations of the North Atlantic and Celtic Sea regions, than for the climate zones considered in Table 4; again, `tas` shows the most obvious fixed effect.

Table SM2 of the SM estimates a LMM for change Δ^Q of annual minima from global and climate zones, and similarly Table SM4 estimates a LMM for change Δ^M in the annual means for global and climate zones. Table SM4 illustrates clearly that changes Δ^M in annual mean are more predictable than changes Δ^Q of annual spatial maxima in Table 4, even for `sfcWind` and `sfcWindmax` in the Temperate North and Arctic zones. However, the magnitudes of the changes Δ^M in wind variables (see Table SM3) are very small.

5.3. Concluding remarks

As noted in Section 1, climate model output requires calibration to spatio-temporally local conditions to reduce its bias and potentially its variance. Given the obvious absence of measurement data for the future to 2100, any calibration is problematic, requiring the assumption that the characteristics of the estimated calibration model persist into the future. In this work we choose not to calibrate, preferring to estimate *changes* in key distributional characteristics of the climate variables directly from the climate model output. Diagnostic plots for GEVR (Figures 6 and 7, and those of Section SM5) suggest that when present, climate-related changes in 100-year return value are generally explainable by a change in GEVR location parameter (i.e. μ^1) rather than changes in tail characteristics (σ^1 and ξ^1).

It is important to consider why obvious climate effects in both annual mean differences Δ^M and return value differences Δ^Q are visible in global and climate zone annual means and extremes for `rsds` and in particular `tas`, but not for wind variable `sfcWind` and `sfcWindmax`. Does this reflect inadequacy of the physical climate models for wind characterisation, or a genuine lack of climate effect on spatio-temporal extremes of wind variables? Perhaps the more probable explanation is the limited spatio-temporal resolution of current climate models, which are therefore unable to capture local changes in atmospheric pressure fields driving winds (but see e.g. Ewans and Jonathan 2023 regarding tropical cyclones around Madagascar). Presumably the spatio-temporal scales of climate-related changes to `rsds` and `tas` are considerably larger. It is also interesting to consider why there is most consistency in estimates for the distributions of both Δ^M and Δ^Q for `tas`. Does this indicate that `tas` is inherently easier to forecast in a climate model than other variables, or that more effort has been devoted to modelling `tas` well, or perhaps that different modelling institutions make similar physical assumptions in their climate models regarding `tas`?

For statistical modelling of annual extremes and means of `tas`, particularly under scenario SSP126 and sometimes SSP245, we observe differences in estimates for posterior distributions of the 2015 base year model parameters (μ^0, σ^0,

ξ^0 of GEVR, and α^0, β^0 for NHGR) given GCM and climate ensemble member. These differences, although relatively small, point a level of inadequacy in the assumed linear form for the variation of GEVR and NHGR model parameters in time, and suggests it might be appropriate to consider a non-linear parameter variation (especially for GEVR level μ). An additional step might be to estimate models for all scenarios (using data for a given combination of GCM, climate variable and ensemble member) simultaneously, imposing a common starting tail for the distribution of climate variable in 2015.

Previous studies (e.g. Meucci et al. 2020, Ewans and Jonathan 2023) of climate effects on the return value for significant wave height H_S derived from CMIP5 and CMIP6 output, have claimed more confidence in inferences. For example, in broad terms, Meucci et al. 2020 claims a 10% increase in return values for H_S in the Southern Ocean. Ewans and Jonathan (2023) claims weak effects with climate scenario and location offshore Southern Australia and Madagascar, the trends of which are consistent with Meucci et al. 2020. However, other studies (e.g. Kumar et al. 2015) have found little evidence for trends in extreme wind speeds from climate model output. Nevertheless is important to consider why the current study does not find compelling evidence for climate change effects on `sfcWind` and `sfcWindmax` which drive H_S. One possible explanation is the analysis of annual maxima in the current work, compared with a peaks-over-threshold analysis in the two articles mentioned; although Ewans and Jonathan (2023) also consider some analysis of temporal block maxima and comment on its inefficiency relative to peaks-over-threshold. In the current work, annual maximum analysis was adopted since it provided a straightforward pre-processing route to compile temporal and spatio-temporal block maxima, possibly at the expense of statistical efficiency. Another possibility is that taking maxima over large spatial domains (e.g. over climate zone or the whole globe) has the effect of mixing different extreme value tails together, thereby complicating estimation of tail characteristics. In this situation, it would be advisable to restrict spatial domains so that the locations they contain are likely to exhibit the same tail behaviour. However, results for single location analysis for the North Atlantic and Celtic Sea region also do not show obvious return value trends for wind variables. Another source of increased uncertainty in the current work is our consideration of not only multiple climate models, but also of multiple ensemble runs for those climate models. As shown in Section 5.2, uncertainty in estimating changes in return value is related at least to some degree to variability between estimates from different climate models and their constituent ensembles.

Characterising changes in large-scale spatio-temporal mean characteristics of wind variables (`sfcWind` and `sfcWindmax`), irradiance (`rsds`) and near-surface temperature (`tas`) in output of CMIP6 GCMs is relatively straightforward. Estimating changes in extreme quantiles of the distributions of large-scale spatio-temporal maxima is considerably more challenging. The current analysis shows that CMIP6 output is informative for changes in extremes of annual spatial maxima of `tas` and `rsds` (over large spatial domains and at specific locations in the North Sea and Celtic Sea regions). Further, the effect of climate scenario, climate model and constituent ensemble member variability on the change in 100-year value over the next 100 years can be quantified to a reasonable degree. For `sfcWind` and `sfcWindmax` however, there is less evidence in the CMIP6 output in general supporting changes in return value. Moreover, the observed variability in return value change is dominated by sources other than climate scenario.

Acknowledgements

Appendix A. Bayesian inference

Inference for the GEV regression and NHGR models described in Section 3 is performed using Markov chain Monte Carlo (MCMC, see e.g. Gamerman and Lopes 2006) following the method of Roberts and Rosenthal (2009). This procedure was reported previously in Ewans and Jonathan (2023), but is summarised here for completeness and ease of reference. All the parameters $\boldsymbol{\theta}$ of the model are jointly updated for a sequence of $n_B + n_I$ MCMC iterations. At each iteration, a new set of parameter values is proposed, and accepted according to the Metropolis-Hastings acceptance criterion based on (a) the sample likelihood evaluated at the current and candidate states, and (b) the values of the prior densities for parameters at the current and candidate states. Following n_B burn-in iterations, the Markov chain is judged to have converged, so that the subsequent n_I iterations provide a valid sample from the joint posterior distribution of parameters. Prior distributions were specified as $\xi \sim U(-1, 0.2)$; $\sigma \sim U(0, \infty)$; $\mu \sim U(-\infty, \infty)$. Likelihoods for the models are available from the distributions given in the main text. An appropriate starting solution $\boldsymbol{\theta}_1$ for the MCMC inference was obtained by random sampling from the prior distributions of parameters, ensuring a valid likelihood.

For the first $n_S < n_B$ iterations, candidate parameter values $\boldsymbol{\theta}_k^c$ are proposed (independently) from $\boldsymbol{\theta}_k^c \sim N(\mathbf{0}, 0.1^2 \boldsymbol{I})$ following Roberts and Rosenthal (2009). Thereafter $\boldsymbol{\theta}_k^c \sim (1 - \beta) N\left(\boldsymbol{\theta}_{k-1}, 2.38^2 \Sigma_k\right) + \beta N\left(\boldsymbol{\theta}_{k-1}, 0.1^2/4\right)$, where

$\beta = 0.05$, Σ_k is the empirical variance-covariance matrix of parameters from the past k iterations, and $\boldsymbol{\theta}_{k-1}$ is the current value of parameters. Throughout, a candidate state is accepted using the standard Metropolis-Hasting acceptance criterion. Since prior distributions for parameters are uniform, and proposals symmetric, this criterion is effectively just a likelihood ratio. That is, we accept the candidate state with probability $\min(1, L(\boldsymbol{\theta}^c)/L(\boldsymbol{\theta}))$, where $L(\boldsymbol{\theta})$ and $L(\boldsymbol{\theta}^c)$ are the likelihoods evaluated at the current and candidate states respectively, with candidates lying outside their prior domains rejected.

References

Bellprat, O., Kotlarski, S., Luthi, D., Schar, C., 2012. Objective calibration of regional climate models. J. Geophys. Res. Atmos. 117.

Coles, S., 2001. An introduction to statistical modelling of extreme values. Springer.

Ewans, K., Jonathan, P., 2023. Uncertainties in estimating the effect of climate change on 100-year return period significant wave heights. Ocean Eng. 272, 113840:1–17.

Gamerman, D., Lopes, H.F., 2006. Markov chain Monte Carlo: stochastic simulation for Bayesian inference. Chapman and Hall / CRC, Boca Raton, USA.

GEBCO, 2023. General bathymetric Chart of the Oceans. `https://download.gebco.net`.

Ibarra-Berastegui, G., Saenz, J., Ulazia, A., Saenz-Aguirre, A., Esnaola, G., 2023. CMIP6 projections for global offshore wind and wave energy production (2015-2100). Sci. Rep. 13, 18046.

IOGP Report 662, 2024. Potential climate change effects of metocean design and operating criteria. IOGP, London.

Jonathan, P., Ewans, K., 2013. Statistical modelling of extreme ocean environments with implications for marine design : a review. Ocean Eng. 62, 91–109.

Kumar, D., Mishra, V., Ganguly, A., 2015. Evaluating wind extremes in CMIP5 climate models. Clim. Dyn. 45, 441–453.

Lavoie, J., Bourgault, P., Smith, T., Logan, T., Leduc, M., Caron, L.P., Gammon, S., Braun, M., 2024. An ensemble of bias-adjusted CMIP6 climate simulations based on a high-resolution North American reanalysis. Sci. Data 11, 64.

Leach, C., 2024. Changes over time in the 100-year return value of climate model variables: data. https://github.com/Callum-Leach/Climate-Change-100-Year-Return-Value-Offshore-Engineering-Data.

Leach, C., Jonathan, P., 2024. Changes over time in the 100-year return value of climate model variables: software. https://github.com/sede-open/Non-stationary-climate-extremes.

Lemos, G., Semedo, A., Kumar, R., Dobrynin, M., Akpinar, A., Kamranzad, B., Bidlot, J., Lobeto, H., 2023. Performance evaluation of a global CMIP6 single forcing, multi wave model ensemble of wave climate simulations. Ocean Model. 184, 102237.

Meucci, A., Young, I., Trenham, C., Hemer, M., 2024. An 8-model ensemble of CMIP6-derived ocean surface wave climate. Sci. Data 11, 100.

Meucci, A., Young, I.R., Hemer, M., Kirezci, E., Ranasinghe, R., 2020. Projected 21st century changes in extreme wind-wave events. Sci. Adv. 6, 1–10.

Meucci, A., Young, I.R., Hemer, M., Trenham, C., Watterson, I.G., 2022. 140 years of global ocean wind-wave climate derived from CMIP6 ACCESS-CM2 and EC-Earth3 GCMs. Global trends, regional changes, and future projections. J. Clim. doi:`10.1175/JCLI-D-21-0929.1`.

Miao, H., Xu, H., Huang, G., Yang, K., 2023. Evaluation and future projections of wind energy resources over the Northern Hemisphere in CMIP5 and CMIP6 models. Renew. Energ. 211, 809–821.

Roberts, G.O., Rosenthal, J.S., 2009. Examples of adaptive MCMC. J. Comp. Graph. Stat. 18, 349–367.

Severino, L.G., Kropf, C.M., Afargan-Gerstman, H., Fairless, C., de Vries, A.J., Domeisen, D.I.V., Bresch, D.N., 2024. Projections and uncertainties of winter windstorm damage in Europe in a changing climate. Nat. Hazards Earth Syst. Sci. 24, 1555–1578.

Sung, C.L., Tuo, R., 2024. A review on computer model calibration. Wiley Interdiscip. Rev. Comput. Stat. 16.

Tett, S.F.B., Gregory, J.M., Freychet, N., Cartis, C., Mineter, M.J., Roberts, L., 2022. Does model calibration reduce uncertainty in climate projections? J. Clim. 35, 2585 − 2602.

IPCC, 2013. Climate Change 2013: The Physical Science Basis. Contribution of Working Group I to the Fifth Assessment Report of the Intergovernmental Panel on Climate Change. https://www.ipcc.ch/report/ar5/wg1/.

IPCC, 2021. Summary for Policymakers. In: Climate Change 2021: The Physical Science Basis. Contribution of Working Group I to the Sixth Assessment Report of the Intergovernmental Panel on Climate Change. www.ipcc.ch/report/ar6/wg1/downloads/report/IPCC_AR6_WGI_SPM.pdf.

Waidelich, P., Batibeniz, F., Rising, J., Kikstra, J.S., Seneviratne, S.I., 2024. Climate damage projections beyond annual temperature. Nat. Clim. Chang. 14, 592–599.

West, B., Welch, K., Galecki, A., 2022. Linear mixed models: a practical guide using statistical software. Chapman and Hall/CRC.

Young, I.R., Ribal, A., 2019. Multiplatform evaluation of global trends in wind speed and wave height. Science 364, 548–552.